Technical Report
TR-23-26
March 2024

Criticality effects of long-term changes in material compositions and geometry in disposal canisters with insert Rebus Concept 1 P355N and P460N

Fredrik Johansson
Per Zetterström
Kastriot Spahiu

SVENSK KÄRNBRÄNSLEHANTERING AB

SWEDISH NUCLEAR FUEL
AND WASTE MANAGEMENT CO

Box 3091, SE-169 03 Solna
Phone +46 8 459 84 00
skb.se

SVENSK KÄRNBRÄNSLEHANTERING

ISSN 1404-0344
SKB TR-23-26
ID 2025926
March 2024

Criticality effects of long-term changes in material compositions and geometry in disposal canisters with insert Rebus Concept 1 P355N and P460N

Fredrik Johansson[1], Per Zetterström[2], Kastriot Spahiu[1]

1 Svensk Kärnbränslehantering AB
2 Vattenfall Nuclear Fuel AB

Keywords: Nuclear criticality, Spent nuclear fuel, Reactivity, Corrosion of materials.

This report is published on www.skb.se

Abstract

In an effort to optimise the canister design, SKB is evaluating alternative canister inserts in the so-called Rebus project. A key area is the evaluation of the alternative concepts in their post-closure performance in a final repository. A key issue in the assessment of post-closure safety for a final repository for spent nuclear fuel is the analysis of the reactivity of the fuel over time, with a focus on situations that would imply a high reactivity. It needs to be demonstrated that criticality is avoided in all such situations. In this report the reactivity analysis of a failed canister with altered material and geometrical properties is carried out for the Rebus Concept 1 insert. As in previous work with the reference insert, it is found that the reactivity increase is relatively small and caused mainly by the filling of the gap between the fuel rods and the insert framework with magnetite in the PWR case or all the space outside the fuel channels in the BWR case. Credit for burnup might be necessary for both BWR an PWR fuel, but the results indicate that the magnetite growth will only demand a slight increase of that credit. The final requirement on burnup, or other possible measures of reactivity control, will be determined in the criticality analysis for the final repository.

Sammanfattning

För att optimera kapseldesignen utvärderar SKB alternativa insatser för kopparkapseln inom det så kallade Rebus-projektet. Ett viktigt område är utvärderingen av de alternativa konceptens prestanda efter förslutning i ett slutförvar. En central fråga vid bedömningen av säkerheten efter förslutning av använt kärnbränsle är analysen av bränslets reaktivitet över tid, med fokus på situationer som skulle innebära hög reaktivitet. Det måste visas att kriticitet undviks i alla sådana situationer. I den här rapporten utförs en analys av reaktiviteten i en kopparkapsel som tappat sin integritet med ändrade material- och geometriegenskaper för Rebus-koncept 1-insatsen. Resultaten visar att reaktivitets-ökningarna, främst orsakad av fyllning av utrymmet mellan bränslestavarna och insatsramverket med magnetit i fallet med PWR eller allt utrymme utanför bränsleboxarna i fallet med BWR, för de analyserade scenarierna blir relativt små. Detta är i linje med tidigare arbete med referensinsatsen. Utbränningskreditering kan komma att bli nödvändigt både för PWR och BWR bränslen, men resultaten pekar på att endast en liten ökning av utbränningskrediten skulle behövas. Det slutliga kravet på utbränning, eller andra åtgärder för att begränsa reaktiviteten, kommer att fastställas i kriticitetsanalysen för slutförvaret.

Contents

1 Introduction

Neutrons from radioactive disintegrations can cause nuclear fission in fissile isotopes in the fuel. As long as the canister is intact, the great majority of neutrons generated by these disintegrations will pass out of the fuel without causing fissions. In the case of ^{235}U and ^{239}Pu in particular, the efficiency of the fission process increases if the neutrons are moderated (slowed down) to lower energies by collisions with light atomic nuclei. This could occur if water penetrates a failed canister. New neutrons are released by the fissions, and if more neutrons are formed than are consumed, the process can become self-sustaining. The system is then said to be critical and large quantities of energy can be liberated.

For the final repository the basic requirement concerning margin to criticality is that the effective neutron multiplication factor (k_{eff}) including uncertainties should be less than 0.95 in water-filled canister with intact geometry. In unlikely events/accidents the k_{eff} value can exceed 0.95 but, in all cases, should be less than 0.98 including uncertainties. This issue is discussed further in Section 4.

If water is assumed to leak in, long term chemical processes will change the material compositions and geometries in the canister during the one-million-year analysis period. The main process expected to significantly affect the chemical composition of the materials in the canister is the corrosion of the carbon steel of the insert, the corrosion of the stainless steel, Inconel or Zircaloy in the fuel assembly structural material, the corrosion of Zircaloy cladding and finally the corrosion of spent fuel itself. During metal corrosion, various anoxic corrosion products are formed, invariably with lower density than the metal itself, thus causing a volume increase in the canister, accompanied by geometrical changes. The reactivity effects caused by these changes were analyzed for the reference insert.

The corrosion of the canister materials and the changes in geometry (Fe corrosion products have higher molar volume than Fe) and material composition (Fe is converted to Fe_3O_4) occurring after a canister is breached may affect the reactivity in the long term and need to be accounted for. Recent analysis of this issue for a canister in a repository setup has shown that a small increase in the burnup is necessary to compensate for the increase in reactivity caused by these long-term material and geometry changes (Agrenius and Spahiu 2016). Several UK studies discuss the rapid transient (RT) and Quasi Steady State (QSS) criticality and their relevance for the repository (Baldwin et al. 2016, Hicks et al. 2018) as well as the likelihood and consequences of post-closure criticality in a generic way, given the lack of a deep geological repository site (Winsley et al. 2015, Hicks et al. 2017, Mason et al. 2014).

The current design of the KBS-3 canister for spent nuclear fuel consists of a corrosion resistant copper shell and a cast iron insert providing mechanical strength. This design is referred to as the reference design or the reference canister in this report. There are two versions of the reference insert, one housing 12 BWR fuel assemblies and one housing 4 PWR assemblies, see e.g., Jonsson et al. (2018).

SKB is evaluating alternative canister inserts in the project Rebus, striving to optimise canister design. An important effort is made to propose a canister insert that can be more reliably produced on an industrial scale than the reference canister, while fulfilling the same design requirements as the reference canister concerning e.g. mechanical loads in the repository. Currently (in May 2023), three alternative insert concepts, denoted Concept 1, 2 and 3, respectively, are being considered. In Section 5.1 more details are given for the design of Concept 1.

A key area in the evaluation of the alternative concepts is obviously their post-closure performance in a final repository, including a long-term criticality analysis. As shown in Section 5, Concept 1 differs most from the reference design, and most design efforts have to date been made for this concept. The emphasis in this report is, therefore, on Concept 1 and its two versions based on the steel grade used for their fabrication, P355N and P460N respectively. Concept 2 is a development of the reference design with two major changes; no steel cassette is used for forming the channels and it does not include an integrated base. Concept 3 is geometrically identical to Concept 2 but manufactured from a different material and by a different method. Concepts 2 and 3 are more similar to the reference design and are not discussed further here, but a general evaluation of their performance in the repository is discussed by Hedin[1].

[1] Hedin A, 2023. Post-closure safety evaluations of alternative KBS-3 canister insert designs. SKBdoc 1969342, ver. 1.0. (Internal document.)

The outer dimensions of the three insert concepts are the same as those of the reference insert, and the design of the copper shell that they would be emplaced in is also the same as that of the reference design. Therefore, the performance of the copper shell is generally expected to be the same for all the alternative inserts.

SKB has carried out a preliminary analysis of the criticality with an early design of Concept 1 P355N included in Hedin 2023[2] as well as another analysis of the long-term changes in a disposal canister with the reference insert by Johansson et al[3].

[2] Hedin A, 2023. Post-closure safety evaluations of alternative KBS-3 canister insert designs. SKBdoc 1969342, ver. 1.0. (Internal document.)

[3] Johansson F, Kirkegaard J, Zetterström P, 2019. Kriticitetsanalys för slutförvaring av använt bränsle. SKBdoc 1605532 ver 1.0. (Internal document, in Swedish.)

2 Objective

In this study the criticality conditions are analysed in a canister considering the changes in material compositions and geometries caused by water ingress and long-term corrosion of all the materials.

The purpose is to investigate the reactivity changes caused by these long-term processes and to judge if criticality is reached.

3 Methods

The programme package Scale-6.2.2 has been used for all reactivity calculations with the cross-section library ENDF/BVII.1 252 groups (ORNL_2018). For reactivity calculations Keno-Va has been used, while burnup calculations have been carried out with the code module Triton. The codes have been used as described in the methodology report[4]. All calculations have been carried out with a precision of 10 pcm, i.e., +/− 0.00010.

[4] Kriticitetsanalys och utbränningskreditering-Metodikrapport. SKBdoc 1369704 ver 6.0. (Internal document, in Swedish.)

4 Criticality safety criteria

The acceptance criterion for the calculated effective neutron multiplication factor k_{eff} including the uncertainties is:

- 0.95 for a water-filled canister with intact geometry.
- 0.98 for a water-filled canister in which geometry changes occur due to corrosion of materials.

The use of the higher value for k_{eff} (0.98) is justified because it is used for the unlikely situation when:

1. The integrity of the canister is lost, which the actual safety assessment for the repository (SR-PSAR) shows to be improbable in a time perspective of 1 million years.
2. The carbon steel corrodes to magnetite and/or siderite which expand uniformly in the free space of the canister until reaching a maximum reactivity.
3. Pure water with a temperature of 4 °C fills all the free space in the canister.
4. The increase in the reactivity by the presence of dissolved hydrogen in water and of dissolved actinides deposited in corroding iron surfaces is accounted for.

This reasoning is in line with the argument that 0.98 is used as limit for unlikely events, events of class H3 and H4 for Clab and other Swedish nuclear facilities.

Further, it has been shown that the consequences of a critical event in the spent fuel repository are relatively limited and it does not affect the neighbouring canisters (Hedin et al. 2013).

5 Description of the system

As discussed in the Introduction, the Concept 1 insert is the one which differs most from the reference insert. This report discusses the long-term criticality analysis for Concept 1, and the geometrical and material data used in the calculations will be described in some detail in this section.

Two versions of the Concept 1 insert are discussed, namely Concept 1 P355N and Concept 1 P460N, realised with slightly different carbon steel grades, which results in some differences in the dimensions of the insert. Both versions of Concept 1 consist of a main load bearing component in the form of a seamless cylindrical tube made of fine-grained carbon steel for pressure purposes, an inner carbon steel plate framework within which the fuel is emplaced, carbon steel lid and base plates and graphite sealings between the tube and lid or base plates. The geometrical details of the Concept 1 insert will be described shortly in Sections 5.1.1 and 5.1.2, while the material composition and some more geometrical details are discussed in Sections 5.1.3 and 5.1.4.

5.1 The disposal canister

5.1.1 Canister design with Concept 1 P355N insert

There are two main versions of the Concept 1 (short C-1 in Figures and Tables) insert, one for BWR fuel and one for PWR fuel assemblies, shown in the figures below.

In locations where the inner framework plates terminate against the steel tube, i.e., at the ends of the carbon steel plates, a 1 mm nominal gap exists between the framework and the tube according to preliminary specifications.

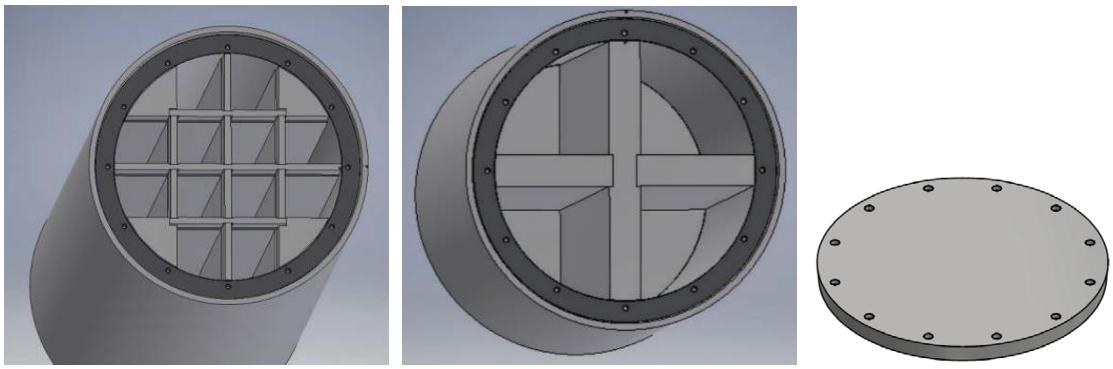

Figure 5-1. *View of the C-1 P355N insert for BWR (left), PWR (centre) and of the lid (right).*

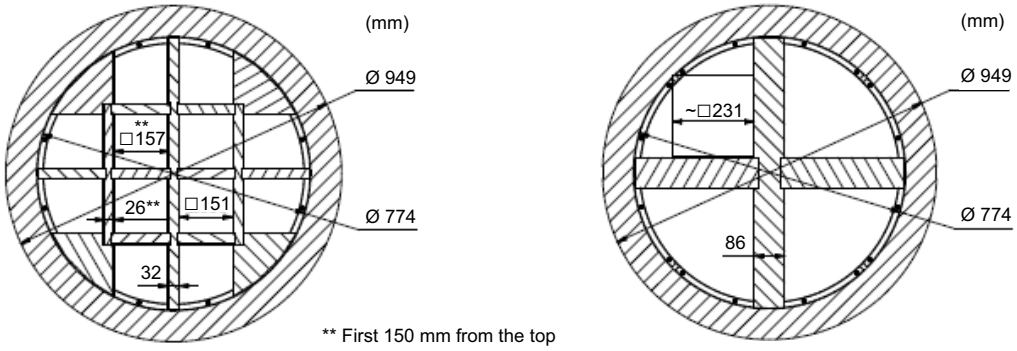

Figure 5-2. *Cross section and some dimensions of the C-1 P355N insert, BWR (left) and PWR (right).*

Some key geometrical data which will be used in this report to calculate the different geometrical arrangements caused by corrosion of all components inside the insert after water contact are summarised in Table 5-1.

Table 5-1. Key geometrical data for the BWR and the PWR versions of Concept 1 P355N (Ronneteg 2023a). All measures in metres.

	BWR	PWR
Tube length	4.573	4.573
Tube outer diameter	0.949	0.949
Tube inner diameter	0.774	0.774
Internal length between base and lid plates	4.461	4.461
Framework plate lengths	4.458	4.458
Framework plate thicknesses	0.032*	0.086
Side length of fuel compartments in framework	0.151**	0.231
Steel lid and base diameter	0.910	0.910
Steel base thickness	0.056	0.056
Steel lid thickness	0.056	0.056

* The dimensions of the corner beams are 175 x 175 mm.

** A width of 0.151 m has been used in criticality calculations for the whole fuel compartment.

5.1.2 The design of Concept 1 P460N insert

The seamless tube of Concept 1 insert with this steel grade is only 70 mm thick instead of 87.5 mm for the Concept 1 insert P355N, meaning that for the same framework volume, the free volume inside of the insert is larger.

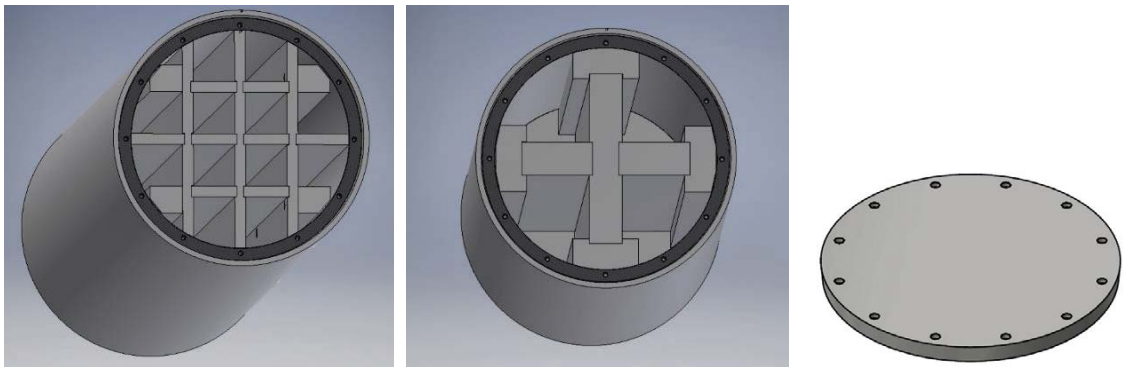

Figure 5-3. *View of the C-1 P460N insert for BWR (left), PWR fuel (centre) and of the lid (right).*

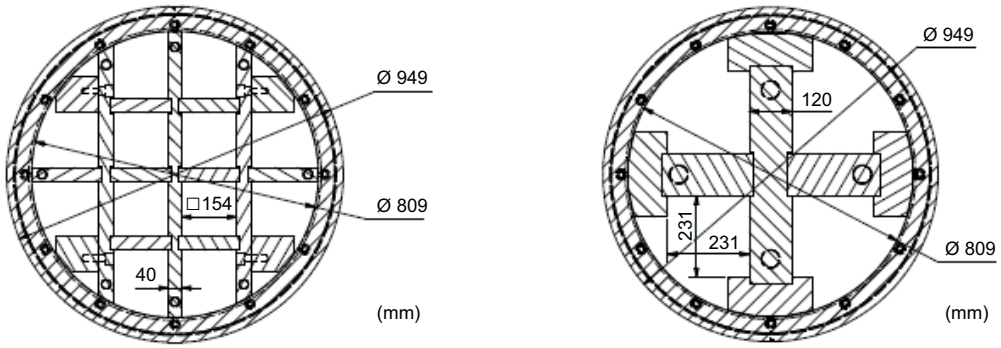

Figure 5-4. *Cross section and some dimensions of the C-1 P460N insert, BWR (left) and PWR (right).*

Table 5-2. Key geometrical data for the BWR and the PWR versions of Concept 1 P460N (Ronneteg 2023b). All measures in metres.

	BWR	PWR
Tube length	4.573	4.573
Tube outer diameter	0.949	0.949
Tube inner diameter	0.809	0.809
Framework plate lengths	4.458	4.458
Internal length between lid and base plates	4.461	4.461
Framework plate thicknesses	0.040*	0.120
Side length of fuel compartments in framework	0.154	0.231
Steel lid and base diameter	0.910	0.910
Steel base thickness	0.056	0.056
Steel lid thickness	0.056	0.056

* The dimensions of the rectangular plates at the corners are 120 × 100 mm.

5.1.3 Some more geometrical data for the Concept 1 insert

The interior surface areas and volumes are as described in Table 5-3, while in Table 5-4 a more detailed specification of free volumes for various compartments of the insert is given. As seen from Table 5-3, the main difference between the Concept 1 inserts and the reference insert is the higher free volume in the fuel-filled canister. In the reference insert the free volume for the fuel-loaded BWR insert is 1 m^3 while for the BWR insert of Concept 1 the free volume is 0.97 m^3 or 1.07 m^3 depending on the steel grade. In the same way, the free volume of the refence PWR insert is 0.7 m^3 while the Concept 1 PWR insert has a free volume of 1.25 m^3 or 0.99 m^3 depending on the steel grade. These free volumes are slightly larger for Concept 1 BWR P460N insert (see Table 5-3), realised with a higher strength grade of carbon steel and thus with a thickness of the large tube of only 70 mm instead of 87.5 mm for the Concept 1 P355N insert.

The presence of this larger free volume in the new insert design and its asymmetrical distribution in the BWR insert (more free volume in the peripheral channels of the canister, see Table 5-4) makes it necessary to assume that the magnetite produced through continuous water corrosion, after reaching the fuel channel (BWR Zircaloy box) wall in the central positions will be distributed in the free space of the peripheral positions instead of entering the space between fuel rods because this is the most penalising situation from a reactivity viewpoint. It cannot be excluded that some magnetite enters the space between fuel rods, but since it is pessimistic to assume that it reaches the space outside the fuel channel in the peripheral positions, a calculation with this assumption is carried out first, see further Section 6.4 and Appendix A.

Table 5-3. Void volumes and internal surface areas in the reference inserts and for the Rebus Concept 1 inserts.

Design	Total void volume, unloaded	Fuel volume	Total void volume, loaded	Area available for corrosion	Reference
BWR P355N	1.368 m^3	12 × 0.033 m^3	0.972 m^3	53.39* m^2	Ronneteg 2023a
PWR P355N	1.544 m^3	4 × 0.074 m^3	1.248 m^3	27.71* m^2	Same as above.
BWR P460N	1.468 m^3	12 × 0.033 m^3	1.072 m^3	57.58* m^2	Ronneteg 2023b
PWR P460N	1.284 m^3	4 × 0.074 m^3	0.988 m^3	39.07* m^2	Same as above
Reference BWR	1.396	12 × 0.033 m^3	1 m^3	35 m^2	Volume: SKB 2022c Area: SKB 2010
Reference PWR	0.996	4 × 0.074 m^3	0.71 m^3	17 m^2	Volume: SKB 2022c Area: SKB 2010

* Assuming a tight lid. If not tight also the outer surface should be added.

Table 5-4. Void volumes in BWR and PWR Concept 1 inserts (Ronneteg 2023a and Ronneteg 2023b).

Design	Central channels	Peripheral up and down channels	Peripheral side channels	Total void volume unloaded
C-1 P355N BWR	4 × 0.102 m^3	4 × 0.120 m^3	4 × 0.120 m^3	1.368 m^3
C-1 P460N BWR	4 × 0.106 m^3	4 × 0.120 m^3	4 × 0.141 m^3	1.468 m^3
Design	**Volume of channels**			
C-1 P355N PWR	4 × 0.386 m^3			1.544 m^3
C-1 P460N PWR	4 × 0.321 m^3			1.284 m^3

5.1.4 Material data for the Concept 1 insert.

The requirements on chemical composition for the framework plates as well as for the steel lid and base are the same for both concept P355N and P460N and are given below in Tables 5-5 and 5-6. The requirements on the chemical composition for the seamless steel tubes differ and are shown in Tables 5-7 and 5-8.

The manufacturing requirements regarding chemical composition of the framework and the lid and base materials are given in Table 5-6 and Table 5-7, respectively. The steel grades for these components are S235J2+N (framework) and P355GH+N (lid and base).

Table 5-5. Requirements on chemical composition of the carbon steel framework material S235J2+N (Ronneteg 2023c[5], SIS 2019).

Parameter/Element (% by mass)	Specification
Carbon (C)	≤ 0.17
Manganese (Mn)	≤ 1.40
Phosphorus (P)	≤ 0.025
Sulfur (S)	≤ 0.025
Copper (Cu)	≤ 0.55

[5] Ronneteg U, 2023c. KBP 3021 – Temporary manufacturing specification – Internal structure – Steel Plate. SKBdoc 1964912 ver. 1.0. (Internal document.)

Table 5-6. Requirements on the chemical composition of the carbon steel lid and base material P355GH+N (Emilsson 2021[6], SIS 2017).

Parameter/Element (% by mass) [a]	Specification
Carbon (C)	0.10 to 0.22
Silicon (Si)	≤ 0.60
Manganese (Mn)	1.10 to 1.70
Phosphorus (P)	≤ 0.025
Sulfur (S)	≤ 0.010
Aluminium (Al) total	≥ 0.020
Nitrogen (N)	≤ 0.012 [b]
Chromium (Cr)	≤ 0.30
Copper (Cu)	≤ 0.05 [c]
Molybdenum (Mo)	≤ 0.08
Niobium (Nb)	≤ 0.040
Nickel (Ni)	≤ 0.30
Titanium (Ti) max	0.03
Vanadium (V)	≤ 0.02
Others Cr + Cu + Mo + Ni	≤ 0.70

a) Elements not included in this table shall not be intentionally added to the steel without the agreement of the purchaser, except for elements which may be added for finishing the cast. All appropriate measures shall be taken to prevent the addition of undesirable elements from scrap or other materials used in the steel making process.

b) A ratio Al/N ≥ 2 shall apply.

c) SKB requirement.

The manufacturing requirements regarding the chemical composition of the steel tubes for the steel grades P355N and P460N are given in Tables 5-7 and 5-8 respectively.

Table 5-7. Requirements on chemical composition of the seamless steel tubes for pressure purposes according to SS-EN 10216-3 (Emilsson and Ronneteg 2022[7], Appendix 1). The two columns refer to alternative, but similar standard qualities of the material P355N (SIS 2013).

Parameter/Element (% by mass) [a]	Specification for 1.0562	Specification for 1.0565
Carbon (C)	≤ 0.20	≤ 0.20
Silicon (Si)	≤ 0.50	≤ 0.50
Manganese (Mn)	0.90 to 1.70	0.90 to 1.70
Phosphorus (P)	≤ 0.025	≤ 0.025
Sulfur (S)	≤ 0.020	≤ 0.010
Chromium (Cr)	≤ 0.30 [c]	≤ 0.30 [c]
Molybdenum (Mo)	≤ 0.08 [c]	≤ 0.08 [c]
Nickel (Ni)	≤ 0.50	≤ 0.50
Aluminium (Altot) [b]	0.020 to 0.040 (≥ 0.020)	0.020 to 0.040 (≥ 0.020)
Copper (Cu)	≤ 0.05 [c, d]	≤ 0.05 [c, d]
Nitrogen (N)	≤ 0.020	≤ 0.020
Niobium (Nb)	≤ 0.05	≤ 0.05
Titanium (Ti)	≤ 0.040	≤ 0.040
Vanadium (V)	≤ 0.10	≤ 0.10
Nb + Ti + V	≤ 0.12	≤ 0.12

a) Elements not included in this table shall not be intentionally added to the steel without the agreement of the purchaser, except for elements which may be added for finishing the cast. All appropriate measures shall be taken to prevent the addition of undesirable elements from scrap or other materials used in the steel making process.

b) Al/N ≥ 2, if nitrogen is fixed by niobium, titanium or vanadium the requirements for Al_{tot} and Al/N do not apply.

c) The sum of the percentage by mass of the three elements chromium, copper and molybdenum shall not exceed 0.45 %.

d) Option 2: In order to facilitate subsequent forming operation, an agreed maximum copper content lower than indicated and an agreed specified maximum tin content shall apply.

[6] Emilsson L, 2021. KBP 3021 – Temporary manufacturing specification – Steel lid and base – Steel Plate. SKBdoc 1964913 ver 1.0. (Internal document.)

[7] Emilsson L and Ronneteg U, 2022. KBP 3021 – Temporary manufacturing specification – Steel Tubes. SKBdoc 1935822 ver 4.0. (Internal document.)

Table 5-8. Requirements on chemical composition of the seamless steel tubes for pressure purposes according to SS-EN 10216-3 (Ronneteg 2022, Appendix 1)[8]. The two columns refer to alternative, but similar standard qualities of the material P460N (SIS 2013).

Parameter/Element (% by mass)[a]	Specification for 1.8905	Specification for 1.8935
Carbon (C)	≤ 0.20	≤ 0.20
Silicon (Si)	≤ 0.60	≤ 0.60
Manganese (Mn)	1.00 to 1.70	1.00 to 1.70
Phosphorus (P)	≤ 0.025	≤ 0.025
Sulfur (S)	≤ 0.020	≤ 0.010
Chromium (Cr)	≤ 0.30	≤ 0.30
Molybdenum (Mo)	≤ 0.10	≤ 0.10
Nickel (Ni)	≤ 0.80	≤ 0.80
Aluminium (Altot)[b]	0.020 to 0.040 (≥ 0.020)	0.020 to 0.040 (≥ 0.020)
Copper (Cu)	≤ 0.05 [c]	≤ 0.05
Nitrogen (N)	≤ 0.020	≤ 0.020
Niobium (Nb)	≤ 0.05	≤ 0.05
Titanium (Ti)	≤ 0.040	≤ 0.040
Vanadium (V)	≤ 0.20	≤ 0.10
Nb + Ti + V	≤ 0.22	≤ 0.12

a) Elements not included in this table shall not be intentionally added to the steel without the agreement of the purchaser, except for elements which may be added for finishing the cast. All appropriate measures shall be taken to prevent the addition of undesirable elements from scrap or other materials used in the steel making process.

b) Al/N ≥ 2, if nitrogen is fixed by niobium, titanium or vanadium the requirements for Al_{tot} and Al/N do not apply.

c) SKB requirement.

The material properties shall comply with the manufacturing requirements in terms of mechanical properties required for the wall thickness T (mm) > 65 to ≤ 80, according to Table 5-9.

Table 5-9. Requirements on mechanical properties of the seamless steel tubes for pressure purposes for wall thickness 65–80 mm.

Mechanical property	Unit	Value	Temperature
Tensile strength, R_m	MPa	490 to 690	Room temperature
Yield strength, R_{eH} or $R_{p.2}$	MPa	> 400	Room temperature
Elongation, l = longitudinal, A	%	> 19	Room temperature
Elongation, t = transverse, A	%	> 17	Room temperature
Impact test, transverse direction, KV2	J	> 27	−20 °C

[8] Ronneteg U, 2022. KBP 3021 – Temporary manufacturing specification – Steel tube P460N. SKBdoc 1985087 ver 2.0. (Internal document.)

5.2 Fuel types

In the current criticality analysis for the final repository of spent nuclear fuel[9] the most reactive fuel types are identified. It is shown that the most reactive fuel assembly type in the disposal canister geometry is W15x15UPGRADE for PWR and SVEA-96 Optima 3 for BWR. These fuel types cover all different fuel types including MOX-fuel and have thus been used as reference fuel types in this study. The reactivity of the spent nuclear fuel varies with time during the 1-million-year analysis period and as shown in Johansson et al.[9], the reactivity for normal fuel types will reach their highest value after about one year of cooling time (i.e., after discharge from reactor).

As in Johansson et al.[9], fresh fuel with 2.3 % U-235 enrichment is assumed for PWR, since this is the limit of enrichment not requiring burnup credit. For BWR 3.4 % enrichment is used, since it is the maximum enrichment allowed in Clab that does not require credit for burnable poison.

To include burnup credit for PWR fuel or credit for burnable poison in BWR fuel, means that higher enrichment fuel is shown to have at most the same reactivity as fresh fuel with the lower enrichment. Credit for burnup or burnable poison will be taken in the complete criticality analysis for the Rebus insert but it has not been taken in this study. More information about criticality analysis with credit for burnable poison in BWR fuel can be found in Kierkegaard[10].

[9] Johansson F, Kirkegaard J, Zetterström P, 2019. Kriticitetsanalys för slutförvaring av använt bränsle. SKBdoc 1605532 ver 1.0. (Internal document, in Swedish.)

[10] Kierkegaard J, 2019. Kreditering av BA i BWR bränsle för kapsel i slutförvar. SKBdoc 1859570 ver 1.0. (Internal SKB document, in Swedish.)

6 Analysis

6.1 Introduction

When loaded in the final repository, the canisters are dry and filled with argon. The k_{eff} in this condition for a canister with Concept 1 insert is shown below for both versions:

Dry canister, P355N

PWR: $k_{eff} = 0.16424$

BWR: $k_{eff} = 0.21328$

Dry canister, P460N

PWR: $k_{eff} = 0.16565$

BWR: $k_{eff} = 0.20547$

The k_{eff} is then calculated for BWR and PWR, assuming that the canisters are filled with water and the geometries of the canister and the fuel intact. In order to be able to model the growth of corrosion products in the insert, the fuel assemblies were assumed here located in the center of their respective channels, in contrast to the criticality analysis for the KBS-3 system and final repository of Spent Nuclear Fuel where the assemblies were placed eccentrically. This is because the reactivity decreases markedly when corrosion products enter between the fuel rods, a situation which occurs much faster with an eccentrical position of the assemblies. In cases such as these discussed in this report, i.e., when long term corrosion of the insert is considered, the most penalizing position of the assemblies is when it is placed as far as possible from all corroding surfaces, i.e., when the fuel assemblies are centred in the channel of the insert.

Water-filled canister, P355N

PWR: $k_{eff} = 0.90772$

BWR: $k_{eff} = 0.94695$

Water-filled canister, P460N

PWR: $k_{eff} = 0.90778$

BWR: $k_{eff} = 0.92134$

In the criticality analysis for the KBS-3 system and final repository of Spent Nuclar Fuel[11] it is shown that k_{eff} is less than 0.95 if the average fuel assembly burnup is higher than 34 MWd/kgU for PWR assuming that both actinides and fission products are considered.

6.2 Water ingress

Water enters the canister when a breach is formed in the copper shell through which water flows into the canister. The scenarios leading to a water-filled canister in repository´s long term evolution are those discussed in the SKB´s most recent safety assessment, SR-PSAR (SKB 2022a). The risk contributing scenarios discussed in SR-PSAR are: a) canister failure due to shear load (in case of a large earthquake in the vicinity of the repository) and b) canister failure due to corrosion (for advective conditions in the bentonite buffer, assumed to be caused by buffer erosion).

[11] Johansson F, Kirkegaard J, Johansson A, 2014. Kriticitetsanalys för KBS-3 systemet och slutförvaring av använt bränsle. SKBdoc 1422106 ver 1.0. (Internal document, in Swedish.)

The calculated mean number of failed canisters due to a large earthquake in the vicinity of the repository at the end of the 1 000 000-year assessment period is 0.079 (SKB 2022a). After the canister shear, it takes a relatively short time (assumed to be 100 y) to have the canister filled with water and the insert and all the metallic parts in the fuel assembly begin to corrode (SKB 2022a, SKB 2022c).

The estimated times of canister failure due to bentonite erosion and subsequent enhanced copper sulphide corrosion are of the order of 100 000 years. This type of failure is assessed to occur only if the few canisters exposed to the most severe flow conditions are also exposed to the highest groundwater sulphide concentrations observed at the site, whereas the overwhelming majority of the canisters are calculated to withstand this failure mode with a margin at the end of the 1 000 000-year assessment period. In this case when the penetration of water occurs, the copper shell has a relatively large damage and thereafter the canister is filled with water. At this point, the corrosion of the insert and other metallic parts in the fuel assemblies starts, as well as fuel dissolution. It should be noted that during such long time periods, changes in the fuel composition due to radioactive decay have to be considered, for example most of the ^{239}Pu has decayed to ^{235}U.

6.3 Long-term evolution of a breached canister

Directly after water contact, simultaneous corrosion of several materials starts and with time will cause changes in the geometry (metals will be consumed and corrosion products with higher molar volume will be produced) and in the material composition of all canister components. This is a complex process which depends on a multitude of parameters, and different geometrical configurations are obtained e.g., if the Zircaloy cladding is completely corroded before or after the filling of the internal free space in the canister with corrosion products. For this reason, here it will be attempted first to evaluate the most probable evolution of the system, i.e., the main evolution case, striving to use realistic corrosion rates for all components under the given conditions and not e.g., conservative upper values to cover for uncertainties, as may be done when release of activation products must be estimated. All conceivable configurations that can be derived from the range of possible corrosion rates for all materials can then be analysed systematically by judging the consequences of a different corrosion rate for a given component. Note that in this report, the term “scenario” is not used in its usual meaning in safety analysis (see for example Section S 3.9 in (SKB 2022a), rather as a synonym for “case” in certain occasions. Thus, for example, carbon steel corrosion rates of 1 μm/year are chosen for the base case, while higher corrosion rates, for example 10 μm/year, are also possible, but, as it will be shown later here, they would just shorten the time to realise the cases analysed here and would not add new cases. This alternative was preferred to the study of all cases obtained by a random combination of corrosion rates within a given interval for all the different materials. During this analysis, special care was devoted to parameter ranges which give rise to scenarios resulting in increased reactivity. Thus, for example, high Zircaloy corrosion rates give rise to scenarios with fuel pellets at the bottom of the channel of the canister, which (as it will be shown in Section.6.4) result in a reactivity decrease. For this reason, calculation cases based on relatively low corrosion rates for Zircaloy were analysed in more detail.

The approach followed here is also to evaluate all conceivable configurations in the canister, while the time at which they are achieved is less important from the reactivity point of view, if all calculations are made with the fuel having the highest reactivity over time. As mentioned before, the reactivity of the spent nuclear fuel varies with time during the 1-million-year period analysed. In order to avoid dependence on this parameter, all calculations are carried out with the highest reactivity of the fuel over time. Further, pure water has been used conservatively in all the calculations, instead of groundwater[12].

Given the complex system under investigation, the reasoning followed here for the less probable system evolutions has been to evaluate their consequences for material configurations which result in increased reactivity. Thus, for example the analysis of the main evolution case assumes in general a long life to the cladding tubes. However, a case when the corrosion of Zircaloy has, for some reason,

[12] Groundwater contains dissolved ions or molecules which can absorb neutrons and this decreases reactivity. Pure water is a good moderator and thus gives the highest possible reactivity.

been faster than what is assumed in the main case, leading to a configuration with fuel pellets at the bottom of the channel of the canister is also included. The consequences of this case have been evaluated for a magnetite layer that has grown until almost touching the fuel rods.

There are several parameters and properties for which there are no published data, or which are difficult to evaluate due to the extremely large time span of the analysis. In this category fall for example the properties of hydrated magnetite, which is indicated as the main component of the outer porous magnetite layer formed on carbon steel and cast iron by most of the experimental studies. In our case we have evaluated the properties of hydrated magnetite, including its density, by using homogeneous mixtures of crystalline magnetite and water. This is expected to be an adequate representation of the position of the nuclei and their interactions with the neutrons in hydrated magnetite, when there are no data in the literature even for the density of this material.

In the following, the long-term corrosion of carbon steel will be discussed first, then the corrosion of metallic parts of the fuel assemblies and of the Zircaloy cladding, always from the point of view of potential material redistribution and geometry changes in the damaged canister.

It should be noted that in this report no credit is taken for manganese in the corroded canister. This is a conservative assumption since manganese lowers reactivity through neutron absorption and will form Mn-oxides, which will mix with the other corrosion products and remain in the canister during the corrosion process.

6.3.1 Long-term corrosion of carbon steel

The corrosion of carbon steel under the anoxic conditions prevailing in the canister interior occurs according to the following reactions:

$Fe(s) + 2H_2O(l) = Fe(OH)_2(s) + H_2(g)$

The ferrous hydroxide produced by this reaction transforms to the thermodynamically more stable product magnetite via the Schikorr reaction:

$3Fe(OH)_2(s) = Fe_3O_4(s) + 2H_2O + H_2$

giving thus the overall reaction:

$Fe(s) + 4H_2O(l) = Fe_3O_4(s) + 4H_2(g)$

The long-term corrosion rate under anoxic conditions is independent of whether or not water is present as liquid or as vapour at high relative humidity (Smart et al. 2002b), thus here it is assumed that the whole surface of the carbon steel at the large tube and the framework, corrodes at constant rate. Several experimental studies have shown the absence of localized corrosion in these materials under repository conditions (SKB 2022b), hence uniform corrosion is assumed to take place during the whole-time interval analysed. This means that the thickness of the corroded layer is assumed equal for all surfaces of carbon steel in contact with water.

The corrosion product magnetite is reported to consist of two layers: a thin, strongly adherent layer and an outer layer of poor adhesion (Smart et al. 2002b). According to these authors, the adherent layer is formed directly on the surface of the metal by reaction (1), while the looser layer is probably formed by the precipitation of dissolved Fe(II) ions. The adherent layer forms very quickly and then does not increase further in thickness, while continuing corrosion leads to the thickening of the non-protective layer. The corrosion rate is controlled by ion transport through the adherent layer and is expected to continue at constant rate over long periods of time.

The density of magnetite is lower than that of the metal, meaning that corrosion of the carbon steel insert will be accompanied by a volume increase. The density of crystalline magnetite (formed for example by high temperature iron oxidation) is reported in literature as 5.17 g/cm^3 (CRC 2012). The volume increase of magnetite in comparison to the volume of carbon steel used to produce this quantity of magnetite, or the Pilling-Bedworth ratio ($R_{P\text{-}B}$) (Pilling and Bedworth 1923), is 2.1, as discussed by Agrenius and Spahiu (2016).

The R_{PB} value for other potential corrosion products formed under reducing conditions as for example $Fe(OH)_2$ are higher, of the order of ~3.7, hence a volume increase of the corrosion products as compared to the corresponding volume of corroded carbon steel of 2–4 times has to be expected. The same holds for other potential corrosion products which may form under reducing conditions, such as green rust or siderite. As mentioned above, most of the magnetite produced in the non-protective layer is very probably a hydrated form of magnetite, less compact than crystalline magnetite.

The mechanical properties of the corrosion product magnetite formed at low temperature (Smart et al. 2001b) are due to its higher proportion of water (Smart et al. 2006a), in contrast to the situation in concrete, where the supply of water is limited, or the oxide films formed at high temperature, which have a much higher hardness and lower water content.

In this chapter we have used the hypothesis based on the results of (Smart et al. 2006a) that the magnetite formed in the region between copper and carbon steel will extrude in the free space in the canister, instead of causing a deformation of the copper shell. Even in other cases, when magnetite is formed in confined spaces for example between the framework plates and the fuel channel (BWR Zircaloy box), it has been assumed as more probable that the magnetite will extrude and fill the available free space, causing no or only a limited deformation of the fuel channel. In general, in such cases an indicative calculation of the reactivity of the system was done even for the less probable case, i.e., also for a case when the formed magnetite deforms the copper shell or the fuel channel (Agrenius and Spahiu 2016).

The same holds for the distribution of the corrosion products during time spans of tens or hundreds of thousand years, for which no experimental or archaeological data exist. The same arguments based on expert judgement as in (Agrenius and Spahiu 2016) are used here, i.e., the magnetite layer is assumed to continue to grow on carbon steel surface and not fall off. However, a calculation for the other variant (magnetite falls off) was also carried out.

The corrosion rate of carbon steel in a damaged canister under repository conditions is one of the most important parameters in evaluating the future evolution of the canister interior. An analysis of this issue was made in 2016 (Agrenius and Spahiu 2016), here some more recent studies on corrosion of carbon steel under near neutral conditions will also be discussed. The corrosion of carbon steel under anoxic conditions has been investigated mainly by waste management organisations due to its use as canister material. In SKB´s program, the corrosion rate of carbon steel was based on the experimental studies by (Smart et al. 2001a, Smart et al. 2002a, 2002b) in synthetic groundwater. The corrosion rate was shown to be independent of both hydrogen gas pressure and Fe(II) concentration in solution. Practically no difference was observed in long term corrosion rates of carbon steel and cast iron. The long-term corrosion rate is independent of whether or not the water is as a liquid or as vapour at high relative humidity. The mean corrosion rates were low and generally less than 1 µm/year. The measured rates span nearly two orders of magnitude, although most data indicate a rate of less than 0.1 µm/year (SKB 2022b).

In another series of studies of carbon steel corrosion under anoxic conditions in the presence of bentonite clay, slightly higher corrosion rates were observed (Smart et al. 2004, Smart et al. 2006b, Smart et al. 2008), as well as adsorption of large quantities of iron ions in the bentonite. Most of the corrosion rates measured in the presence of the bentonite were of the order of 1–2 µm/year after one year, even though a decrease of the corrosion rate with time is always observed also in these tests.

In a review of corrosion rates for carbon steel under repository conditions, Diomidis (2014) selects a long-term corrosion rate of 2 µm/year for carbon steel under Opalinus clay conditions and a range of corrosion rates between 0.1–5 µm/year.

In his review of anoxic corrosion of carbon steel, King (2008) states that there is a significant body of evidence from well conducted experiments that indicate an anaerobic corrosion rate of the order of 1–2 µm/year in systems containing compacted clay, while in bulk solution long term corrosion rates are of the order of 0.1 µm/year. The decrease of corrosion rate with time is due to the formation of a corrosion layer which tends to be thinner and more compact in bulk solution. Sorption and incorporation of Fe(II) in bentonite clay affects the corrosion layer formed on the metal surface.

Swanton et al. (2015) summarize literature data on anaerobic corrosion of carbon steel in neutral solutions in their Table 8. The corrosion rates are in the range 1–100 µm/year (Sidborn 2018). The corrosion rate in neutral solutions seems to be insensitive to temperature, based on data of Jelinek and

Neufeld (1982). Swanton et al. (2015) observe that short term electrochemical measurements give much higher corrosion rates than long term weight loss or hydrogen evolution measurements. The long-term corrosion rates are plotted in their Figure 8 and span a much lower range, 1–18 µm/year.

In situ corrosion rates of carbon steel in compacted bentonite at Mont Terri (Smart et al. 2017) derived from weight loss measurements after 1.7 years were 1.2–3.4 µm/year, in agreement with other data in the presence of bentonite clay.

A large number of archaeological objects corroded under anoxic conditions has been analysed with different methods, both by SKB (Smart and Adams 2006) and by others (Neff et al. 2006, 2010, Saheb et al. 2008, 2009, 2010, 2011, 2012, Yoshikawa et al. 2008). The corrosion rates for iron objects corroded under anoxic or reducing conditions are in the range 0.1–2 µm/year. Yoshikawa et al. (2008) investigated more than 1 500-year-old iron objects by X-ray computer tomography and estimated corrosion rates in the range 0.1–1.1 µm/year. In many of these objects, thick corrosion layers are observed, and, in many cases, concretion is commonly formed around iron objects, by iron corrosion products mixing with material adjacent to the iron. It is predominantly composed of $CaCO_3$, which undergoes ion exchange with the iron ions released by corrosion to form $FeCO_3$ and other iron compounds. The structure of the concretion is different depending on whether it is exposed to seawater or buried in sediment. In buried conditions the concretion contains predominantly Fe_3O_4, compared to FeOOH and Fe_2O_3 in exposed-to-air situations. It seems highly probable that thick layers of corrosion products can be formed on the surface of the carbon steel. As discussed in (Saheb et al. 2012), the corrosion rates estimated for 500-year-old archaeological objects are of the same order of magnitude (0.6–2 µm/year) as for short term corrosion experiments, suggesting that the presence of the thick corrosion layer does not significantly influence the process.

Based on several reviews of carbon steel corrosion under repository conditions (King 2008, Feron et al. 2009, King et al. 2014, King 2014, Swanton et al. 2015), as well as the data of Smart et al. (2004, 2006b, 2008, 2017) in the presence of bentonite and the archaeological studies mentioned above, a corrosion rate of 1 µm/year seems the most reasonable choice for discussing the main evolution case of a damaged canister.

However, the consequences of a lower corrosion rate, e.g., of the order of 0.1 µm/year, may be considered in calculation cases with such rates, for example to investigate the contribution of fissile material deposited on magnetite. Given that 0.1 µm/year is the lowest limit of corrosion rate range reported in archaeological studies, corrosion rates lower than this value for carbon steel have not been considered.

The same approach as in Agrenius and Spahiu (2016) will be used for hydrated magnetite or other potential anoxic iron corrosion products such as siderite and mackinawite within this chapter.

6.3.2 Potential formation of other anoxic corrosion products

Siderite, $FeCO_3(s)$ is usually formed in groundwaters with relatively high carbonate concentrations through the reaction:

$$Fe(s) + HCO_3^- + H^+ = FeCO_3(s) + H_2$$

In addition, green rust type phases (double layer mixed Fe(II)/Fe(III) hydroxides) may form, but they are metastable with respect to magnetite and siderite in the long term and are not discussed further here.

At relatively high concentrations of sulphide, various forms of iron (II) sulphide compounds may form as corrosion products:

$$Fe(s) + HS^- + H^+ = FeS(s) + H_2$$

In an experimental study of the corrosion of carbon steel by aqueous hydrogen sulphide at low temperatures (Shoesmith et al. 1980), the formation of up to three iron monosulphide phases is reported: mackinawite (tetragonal $Fe_{1+x}S$), cubic ferrous sulphide and troilite (stoichiometric hexagonal FeS). At pH over 6, only mackinawite was formed as corrosion product and will be discussed further here. The concentrations of sulphide in Forsmark are in the range $10^{-4} – 10^{-6}$ M, i.e., relatively low to cause substantial sulphide corrosion. Because of the large defect in both analysed scenarios, large amounts of hydrogen are expected to be produced in the damaged container and, especially in

the erosion/corrosion case, the microbial reduction of sulphate by SRB (Sulphate Reducing Bacteria) using the hydrogen is a possibility. The utilisation of hydrogen by SRB was considered as the cause of the fast iron corrosion, but this hypothesis has been questioned lately (Enning and Garrelfs 2014). In 2004 experimental evidence was presented for a novel corrosion mechanism, in which microbial reduction of sulphate was carried out through direct consumption of iron derived electrons through the semiconducting sulphide layer, without involving hydrogen as an intermediary (Dinh et al. 2004). Without going into details, we point out the following: Chemical microbially influenced corrosion (CMIC) of iron by hydrogen sulphide from microbial sulphate reduction occurs with "natural" organic substrates. There are certain SRB strains which corrode iron by direct utilisation of the metal itself, through a direct electron uptake in the microbe (EMIC). Further, different corrosion products are formed by CMIC (only sulphide) and EMIC, a mixture of iron carbonate (siderite) and sulphides (ca 25 %, mainly mackinawite). The corrosion rates involving microbial corrosion are usually high, as noted in the MiniCan 3 field experiment (Smart et al. 2012) where extensive sulphide corrosion was observed.

The sulphate concentrations in Forsmark vary during the 1 000 000-year analysis period between 0.15 mM to 5 mM during the temperate period, but decrease substantially during the glaciation period (Salas et al. 2010, Joyce et al. 2015). In any case, even by assuming an average concentration of sulphate of 5 mM for the groundwaters in Forsmark, together with the highest predicted flow through a deposition hole during the whole analysis period, around 1.5 moles of sulphide per container and year can be produced by assuming complete microbial reduction of all sulphate. This means that mass balance calculations allow calculating a maximum amount of iron sulphide that can be present as corrosion product in the container, where magnetite will anyhow dominate (see Appendix C). In this estimation, any consumption of sulphide by copper (highly probable, especially in the case of a shear failure, when most of the copper shell is present) has been neglected. At the same time, enough reductant (e.g., H_2 produced by iron corrosion or organic matter) has been assumed to be available for the microbes to convert 1.5 moles of sulphate into sulphide. The reduction of one mole sulphate consumes 4 moles of hydrogen:

$$SO_4^{2-} + 4H_2 + H^+ = HS^- + 4H_2O$$

The sulphide corrosion process produces one mole H_2 per mole FeS(s) produced, so the molar ratio of magnetite to sulphide if only hydrogen produced by iron corrosion is used as reductant is 3:1. This corresponds to a maximum of 10.9 wt% mackinawite in the mixture. As can be seen in Appendix C, full reduction of all sulphate passing through the canister during one-year results in higher mackinawite contents, because we could not exclude the contribution of organic matter.

The formation of siderite with the predicted carbonate concentrations during Forsmark groundwater evolution seems also less probable; a potential pathway may anyhow be through EMIC corrosion or through concretions formed by interaction of magnetite with groundwater (Smart and Adams 2006). Further, the maximum amount of siderite than can be formed during the corrosion of the carbon steel insert of a KBS-3 container may be estimated from the carbonate/bicarbonate concentration in the groundwater and an assumed high flow through the container. The carbonate concentrations in Forsmark vary during the 1 000 000-year analysis period between 0.23 mM to 6 mM depending on the climate conditions (Salas et al. 2010, Joyce et al. 2015). Assuming an average total carbonate concentration of 6 mM in the groundwater during the whole period and a groundwater flow of 300 l/year through the deposition hole, a maximum of 1.8 moles of carbonate salts per container and year can be produced. The amount of the siderite in the siderite-magnetite mixtures is estimated following two different assumptions, see Appendix C.

To investigate the influence of such corrosion products in the container reactivity, calculation cases assuming partial formation of mackinawite or siderite as corrosion products have been carried out. We have carried out the calculations with siderite and mackinawite for the corrosion product configuration which results in high reactivity, i.e., when the corrosion layer approaches the fuel rods for the PWR insert, or when the whole free space outside the fuel channels (BWR Zircaloy box) is filled with corrosion products, but there is water between the fuel rods for the BWR insert (Section 6.4.2).

For siderite, using a theoretical density of 3.87 g/cm^3, the Pilling-Bedworth ratio is 4.2, i.e., the corrosion layer just touches the fuel rods when much less iron has corroded then when the corrosion product is magnetite. The volume of iron needed to corrode in order to produce 1 m^3 of siderite is 1/4.2 = 0.238 m^3 and the situation of a completely filled space in the container may be achieved about twice as fast as when the corrosion product is magnetite.

There are several iron sulphide phases which may form during iron corrosion in the presence of high sulphide concentrations. Experimental studies (Shoesmith et al. 1980), as well as archaeological studies report formation of mackinawite ($Fe_{1+x}S$, x = 0 − 0.1) under the experimental conditions similar to the ones expected in the repository. By using a density of 4.3 g/cm^3 and a molecular weight of 84.7 g/mol, the Pilling-Bedworth ratio for crystalline mackinawite is 2.76. From this, the layer of iron which is corroded when mackinawite touches the fuel rods and the volume of iron needed to be corroded to fill a BWR or PWR canister with mackinawite can be estimated.

6.3.3 Corrosion of Zircaloy and stainless steel

As mentioned before, at the same time as the canister is filled with water and the corrosion of carbon steel starts, the corrosion of Zircaloy cladding tubes as well as the corrosion of spacer grid plates, top and bottom plates and other metallic parts in the fuel assemblies starts.

The corrosion of Zircaloy at relatively low temperature (20–80 °C) proceeds at such low rates that it is impractical to conduct meaningful corrosion test under any reasonable time period (IAEA 2006). Zircaloy coupons were exposed in two Hanford fuel storage pools for a period of three years, during which water chemistry changes occurred which markedly accelerated corrosion of Al alloy and carbon steel specimens. The Zircaloy specimens maintained their silver appearance and the oxide growth was less than the first interference colour range (20 nm thickness), indicating a corrosion rate less than 7 nm/year (Johnson and Burke 1996). This is why corrosion rate correlations generated at high temperature are used to make estimations for corrosion rates at the lower temperatures, such as those expected under repository conditions. Table 20 in (Gras 2014) summarizes the metal loss rates predicted from 10 corrosion models of Zircaloy derived from high temperature data and published from 1964 to 1998. When these models are used to extrapolate corrosion rates to 20 and 50 °C, values between 10^{-11} and 10^{-4} nm/year are obtained, supporting the statement that it is very difficult to measure such rates experimentally. As discussed in (Shoesmith and Zagidulin 2011), despite the presence of radiation fields associated with the fuel, the redox conditions within a waste canister will remain reducing due to the production of oxidant scavengers Fe(II) and H_2 by iron corrosion. Consequently, the only feasible corrosion mode that could lead to degradation of the cladding is passive corrosion. A corrosion rate of 5 nm/year is considered as base case for estimating activation product releases. As discussed before, the lower corrosion rate interval is more interesting for this study. The corrosion rates of Zircaloy in granitic groundwaters at temperatures around 20 C are very likely to be as low as 1–2 nm/year (Gras 2014, Shoesmith and Zagidulin 2011, SKB 2022b).

In spite of the limited thickness of the Zircaloy cladding (less than a millimetre), it is expected to have enough un-corroded metal for time intervals of the order of a few tens of thousands of years to assure their mechanical stability until all the free space in the canister is filled with magnetite. With a corrosion rate of 1 µm/year and the internal carbon steel surface of the BWR P355N or P460N inserts (Table 5-3), the time needed to corrode a volume of carbon steel which causes the complete filling of the free space in the insert with crystalline magnetite is less than 24 000 years. Of course, in the case of hydrated magnetite, which is less dense, or any other anoxic corrosion product as for example $Fe(OH)_2$(s), this time will be shorter. To bound from the other side, when the corrosion of carbon steel proceeds at 0.1 µm/year, the free space inside the 4 BWR and PWR canister variants discussed in this report will be filled with magnetite in time intervals of the order of 156 000–240 000 years. Even at such time spans, the Zircaloy cladding is not expected to have corroded completely, if Zircaloy corrosion rates are of the order of 1 nm/year. In any case, a calculation case with higher corrosion rate for the Zircaloy cladding resulting in its complete corrosion and the accumulation of fuel pellets at the bottom of the channels of the canister has also been carried out. As can be seen in next section, this case results in lower reactivity as compared to the case when the fuel pellets remain inside the Zircaloy cladding, hence no further analysis of the consequences of higher Zircaloy corrosion rates has been undertaken here.

Corrosion of the stainless steel and Inconel structural parts of the fuel assemblies is expected to occur more slowly, probably at 10 to 100 times lower rates than that of the carbon steel under the same conditions, based on several literature data discussed for example in (SKB 2022b). The potential for localized corrosion under the anoxic and reducing conditions expected in the repository is relatively small as discussed in (SKB 2022b), based among others on the data of (Kursten et al. 2004). Under anoxic conditions (Wada et al. 1999) measured very low corrosion rates (< 0.01 µm/year) of 304 SS stainless steel, the material of the hull-end pieces of the fuel assemblies, in seawater-based groundwater

of pH 10. Smart et al. (2004) report anaerobic corrosion rates of stainless steel in alkaline environments in the range of 0.01 to 0.1 μm/y. The corrosion rates under anoxic conditions in alkaline environments were found to be relatively insensitive to pH within the range 6.4 to 13 (Blackwood et al. 2002). Recent data from Sakuragi et al. (2016) and Sakuragi (2017) indicate for corrosion rates of stainless steel under anoxic conditions, both under alkaline pH and in distilled water below 1 nm/y. The measurement of hydrogen generation both in sealed ampoules (Sakuragi 2017) and in a novel approach with determination of hydrogen concentration in the flushing gas (Sakuragi et al. 2016) indicates corrosion rates during the first year of the order of 0.4 nm/y.

A specific part of the fuel assemblies are the grid spacers, made of Zircaloy or Inconel, which are usually thinner than the other parts and may be consumed faster, especially in the case of Inconel. The corrosion of grid spacers could affect the geometry of the fuel rods in a fuel assembly. The effect is expected to be limited, because the grid spacers are not expected to have corroded significantly during the few tens of thousands of years it takes to fill the space between the fuel rods with magnetite. The case that would be the first to experience effects of grid spacer corrosion is BWR fuel assemblies with the part length rods. Calculation cases for this situation have been carried out in (Agrenius and Spahiu 2016), a summary of which can be found in the next sections.

6.3.4 Corrosion of spent fuel

As soon as the canister is filled with water, the corrosion of the spent fuel also starts. In the first period, the release of the IRF (Instant Release Fraction) occurs, consisting of the release of a few percent of the inventory of volatile fission products such as Cs and I. Under the reducing conditions created by the anoxic corrosion of iron, the dissolution rate of spent fuel matrix is expected to occur with an average rate of 10^{-7}/year (SKB 2022a, 2022b, 2022c). This corresponds to an amount of around 3.46 kg U dissolved during for example the 17 300 years needed to fill the BWR insert void with iron corrosion products. As discussed in SR-PSAR (SKB 2022a), this oxidized uranium is expected to be reduced and precipitated as secondary UO_2(s) on the surface of the corroding carbon steel. Evidence for the reduction of oxidized U(VI) on the surface of corroding iron is ubiquitous, both from experimental studies related to geological disposal (Grambow et al. 1996, Cui and Spahiu 2002) and in studies of removal of uranium using zero-valent iron (Fiedor et al. 1998, Gu et al. 1998, Farrell et al. 1999). Recently it was shown that uranium reductive precipitation occurs even in the presence Ca-uranyl-carbonate complexes in the groundwater (Hansson et al. 2023). In solution only a small amount of uranium, corresponding to the low solubility of UO_2(s) under reducing conditions (3×10^{-9} M or 7.5×10^{-7} g/l), is expected to be found. Given that preliminary calculations indicated a slight increase in reactivity due to this redistribution of uranium, the amount of uranium dissolved and deposited on the magnetite layer was estimated for the lower corrosion rate of carbon steel (0.1 μm/year), resulting in longer time periods (72 000 years to corrode 7.2 mm steel) and larger quantities of redistributed uranium (14.4 kg in this case). The dissolution of the fuel matrix is assumed to occur congruently, i.e., the fission products (such as lanthanides) and the actinides (such as e.g., Np and Pu), which are distributed homogeneously in the matrix, are released together with U. Calculations to consider these effects have been carried out, see Section 6.4.9.

6.4 Evolution in time of a damaged canister

6.4.1 Main evolution scenario

The reactivity changes during a scenario evolution involve many phenomena which often contribute in different directions and it is not always evident which one has the strongest influence on reactivity. A change in material will have effects on at least: neutron absorption, moderation, leakage between assemblies, reflection. To see what effect is strongest you often have to make a calculation of the collective behaviour.

First, the canister is assumed fully flooded, i.e. all empty spaces in the canister are filled with water. When steel starts to corrode into magnetite, which has a lower density than steel, it will partly replace the water outside the fuel lattice, but within the walls of the framework. Since magnetite is a better neutron reflector than water and also has lower neutron absorption, the reactivity will increase and will continue to increase until the magnetite reaches the fuel lattice. When the magnetite enters the

fuel lattice it will replace water which in this part of the geometry is needed to moderate the neutrons to enable fission, therefore the reactivity will decrease and continue to decrease the more water is replaced by magnetite.

As discussed above, the corrosion will take place on surfaces that are exposed to water. The growth of magnetite will decrease the gap between the compartment wall and fuel rods. The reactivity effect of this gap decrease is shown in Figure 6-1a for PWR Concept 1 P355N insert and in Figure 6-1b for Concept 1 P460N insert. If the initial distance between the framework plate and the fuel assembly is denoted A, the depth of corroded iron is denoted X, then the gap denoted G is calculated with the formula:

$$G = A - (2.1 \times X - X)$$

For PWR fuel the reactivity behaviour follows the same pattern as in the analysis carried out in (Agrenius and Spahiu 2016).

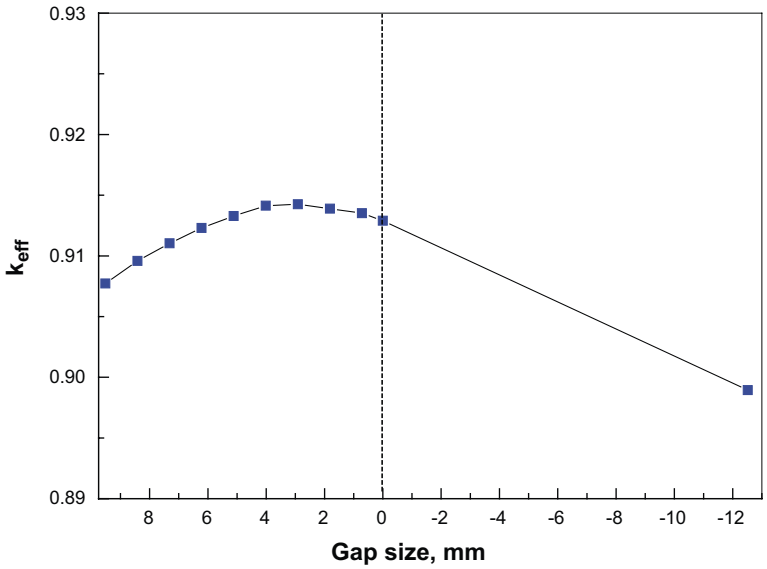

Figure 6-1a. *Calculated k_{eff} vs gap size for a PWR P355N canister. The growth of the magnetite layer into the assembly between the fuel rods has been represented with negative values for the gap size.*

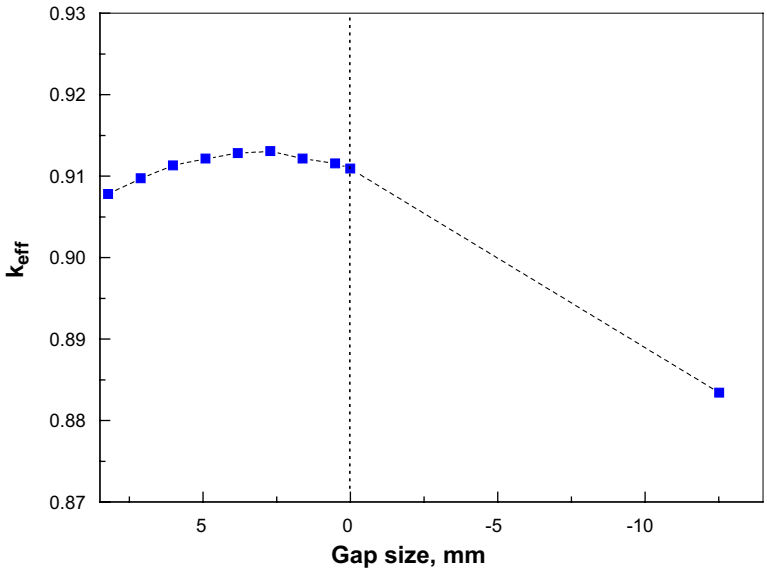

Figure 6-1b. *Calculated k_{eff} vs gap size for a PWR P460N canister. The growth of the magnetite layer into the assembly between the fuel rods has been represented with negative values for the gap size.*

For both PWR P355N and P460N inserts it can be seen that the maximum reactivity (k_{eff} = 0.914 respectively 0.913) occurs when the layer of magnetite has grown and the gap between the magnetite and the fuel rod surface is around 2–3 mm. The space in-between the fuel rods and the gap are still water-filled. This corresponds to the corrosion of a carbon steel layer of about 6 mm (this would give a 12.6 mm corrosion layer thickness assuming the density of crystalline magnetite and thicker layer if hydrated magnetite or other anoxic corrosion products are formed). The assumption made here is that the magnetite formed does not move or fall down in the channel of the canister, but remains on the walls of the insert, as discussed before. Given the large defects in the copper shell in both the shear load scenario and erosion/corrosion scenario, the presence of a sufficient quantity of water to cause corrosion has been assumed here. Continued growth of the magnetite layer will result in a reactivity decrease when the magnetite layer continues growing into the fuel assembly between the fuel rods (this is represented in Figure 6-1a, b with negative values for the gap size).

These calculations were also done for the BWR-case. Note that BWR-fuel bundle is placed in a fuel channel (Zircaloy box) and the magnetite layer will grow against the wall of the fuel channel. It became clear in the early stages of this project that due to the unsymmetrical distribution of the free space in the Rebus insert (more free space in the peripheral positions) that the surplus magnetite produced after the magnetite layer touches the fuel channel in the central positions may enter between the fuel rods in the central positions and decrease the reactivity. Alternatively, it may move to fill the free space in the peripheral positions until all the free space outside the fuel channels is filled. The second alternative is more penalizing and, even if in reality both possibilities may occur simultaneously, in this report it was assumed that all surplus magnetite fills the free space outside other compartments of the insert. Only after reaching this configuration (i.e., all the space outside the fuel channels filled with magnetite, but only water between the fuel rods inside the fuel channels) further iron corrosion will cause magnetite to enter between fuel rods. This configuration, with magnetite filling all the compartments of the insert but not between the fuel rods, causes the sharp increase of reactivity in the two figures below and is used further in the report as the most reactive configuration for a BWR insert. In the case of the BWR P355N insert this configuration is achieved after the corrosion of 6.33 mm carbon steel to crystalline magnetite while for the BWR P460N insert after the corrosion of 7.45 mm steel from all insert surfaces (see Appendix A).

As can be seen in Figures 6-2a and 6-2b the maximum reactivity (k_{eff} > 0.98 and > 0.96 respectively) occurs when the layer of magnetite has grown, the gap between the magnetite and the fuel channel (BWR Zircaloy box) wall is closed and all the space outside the fuel channel is filled with magnetite. This case corresponds to the corrosion of a carbon steel layer of about 6.33 mm for BWR P355N or 7.45 mm for BWR P460N which produces sufficient magnetite to fill all the free space outside the fuel channel in the insert (see Appendix A for details of the calculations). The geometry of the PWR and BWR cases with maximum reactivity is shown in Figures 6-3 and 6-4.

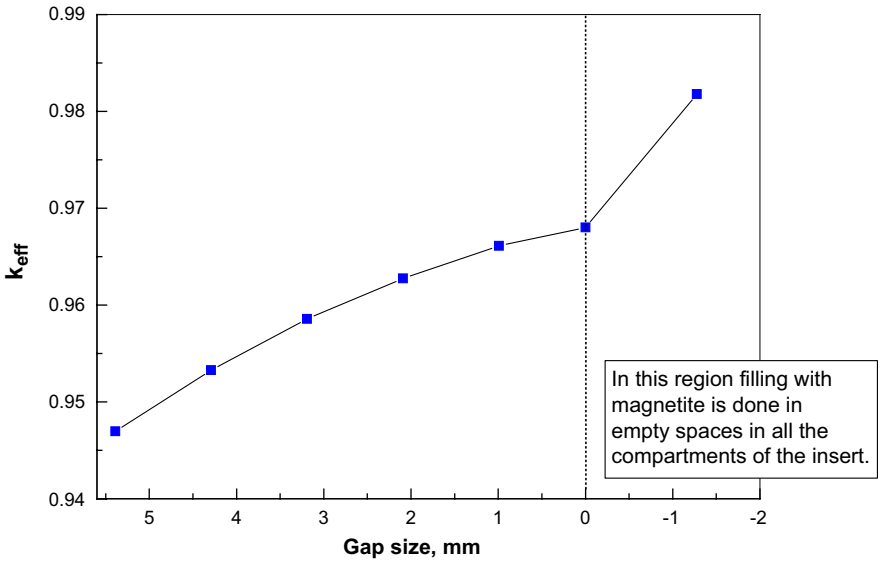

Figure 6-2a. *Calculated k_{eff} as function of the gap size for a BWR P355N canister. The values plotted for negative gap size values correspond to growth of the magnetite layer filling of all the free space in the compartments of the insert outside the fuel channels, with magnetite.*

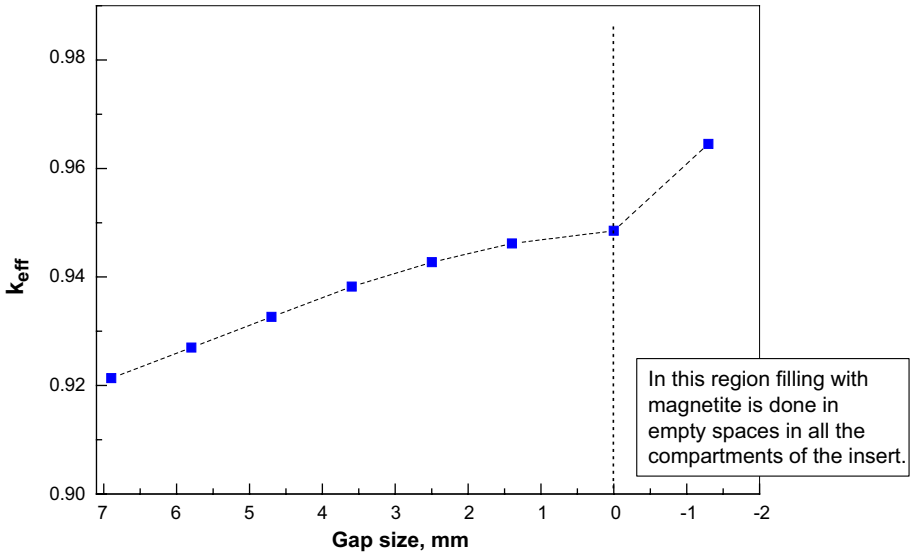

Figure 6-2b. *Calculated k_{eff} as function of the gap size for a BWR P460N canister. The values plotted for negative gap size values correspond to growth of the magnetite filling of all the free space in the compartments of the insert outside the fuel channels, with magnetite.*

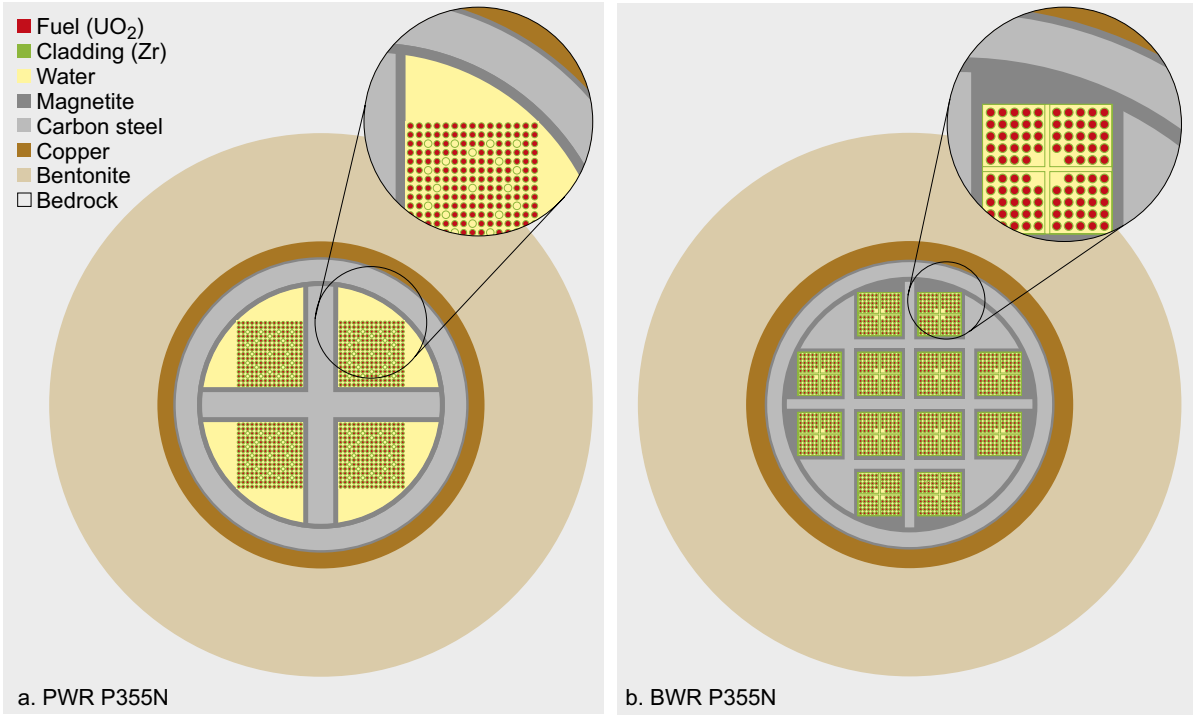

Figure 6-3. *Representation of cross sections of P355N BWR and PWR inserts when the gap between the fuel rods and the insert framework in the PWR case or the whole free space outside fuel channels in the BWR case is filled with magnetite. The area converted to magnetite in the framework plates and in the copper-carbon steel interface is also represented, see magnification.*

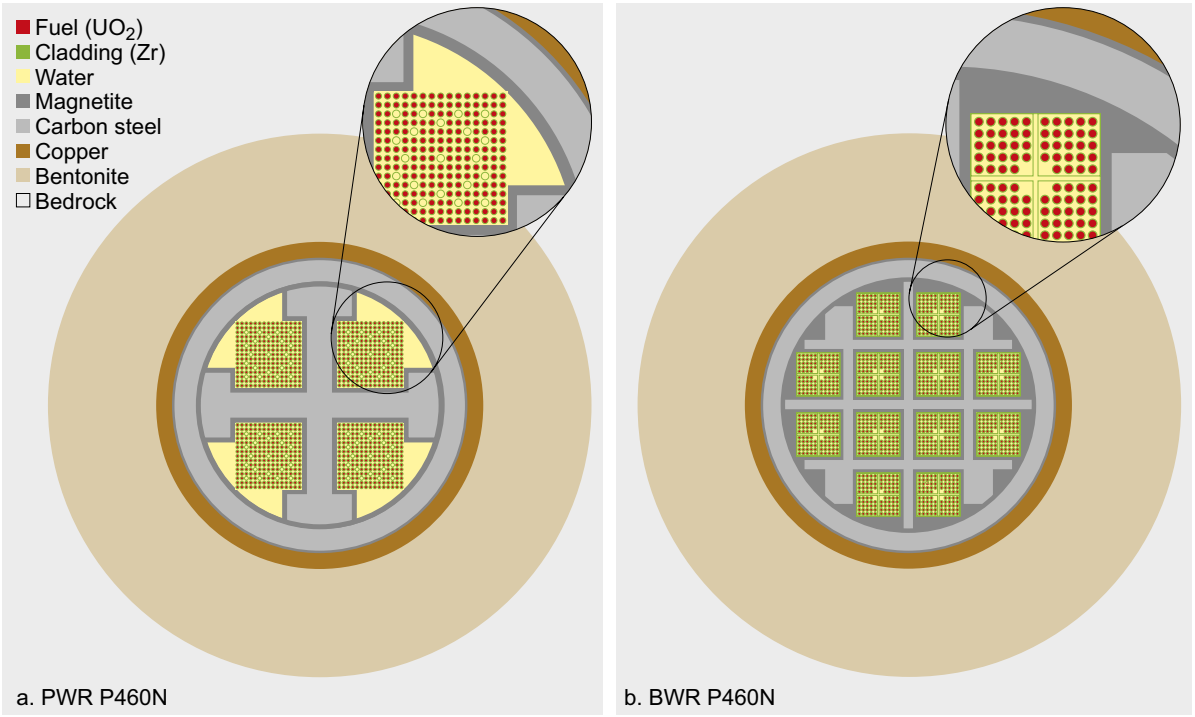

Figure 6-4. *Representation of cross sections of P460N BWR and PWR inserts when the gap between the fuel rods and the insert framework in the PWR case or the whole free space outside fuel channels in the BWR case is filled with magnetite. The area converted to magnetite in the framework plates and in the copper-carbon steel interface is also represented, see magnification.*

All the above calculations were carried out with crystalline magnetite, while the outer porous layer of magnetite formed during carbon steel corrosion is expected to be a solid hydrated to various degrees. There are no data on the properties of hydrated magnetite, and for this reason a sensitivity study of the water content of the magnetite has been done. The reactivity calculations are based on the cases above which give the highest k_{eff}, that is the magnetite layer just touches the fuel rods in the PWR case, and the whole space outside the fuel channels is filled with magnetite in the BWR-case. Water is mixed in the magnetite layer according to Table 6-1 (see also Appendix B on the properties of hydrated magnetite). During the review process, it became clear that the values for 20 wt% and 30 wt% water content correspond to unreasonably high magnetite porosities, hence should be disregarded.

Table 6-1. Density of the hydrated magnetite with various water contents.

Water in the magnetite (weight %)	Density of hydrated magnetite (g/cm^3)	P-B of hydrated magnetite
0	5.17	2.10
5	4.26	2.68
10	3.65	3.57
20	2.82	4.81
30	2.30	6.75

As seen from the table, the $R_{P\text{-}B}$ values of hydrated magnetite increase with hydration causing filling of the gap framework-assembly in the PWR case or of the space outside the 12 fuel channels in the BWR case for a much smaller amount of corroded steel than for crystalline magnetite.

The results of the calculations are shown in Figure 6-5 for the P355N insert and in Figure 6-6 for the P460N insert.

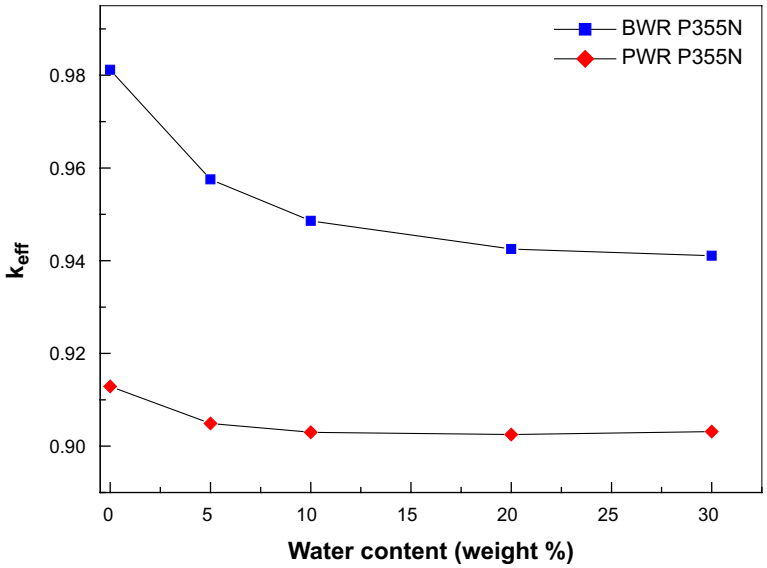

Figure 6-5. *k_{eff} as function of water content in the hydrated magnetite for the P355N insert with magnetite filling the space between the fuel assemblies and the insert framework.*

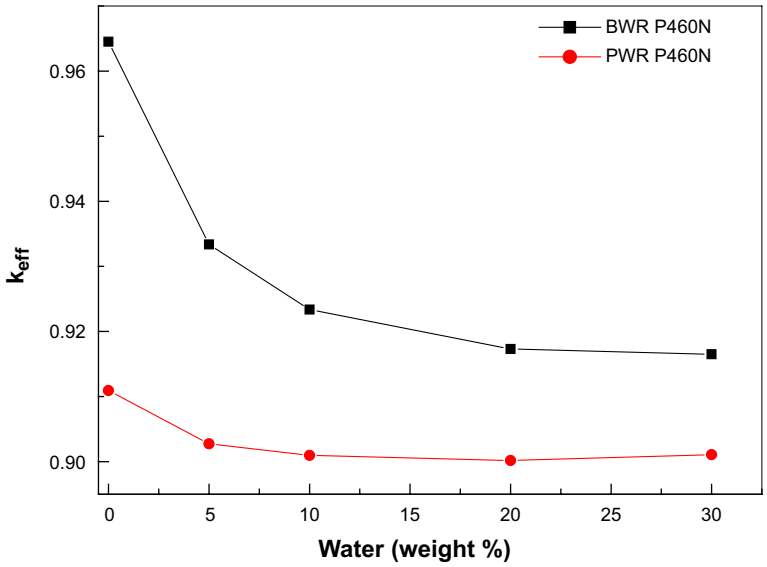

Figure 6-6. *k_{eff} as function of water content in the hydrated magnetite for the P460N insert with magnetite filling the space between the fuel assemblies and the insert framework.*

As can be seen from the figures, the reactivity decreases when water is mixed into the magnetite, i.e., when hydrated magnetite with variable water content is formed as corrosion product instead of crystalline magnetite in the gap between framework plates and fuel rods in the PWR case or in all the free space outside the 12 fuel channels (Zircaloy box) in the BWR case. In this case increasing water content decreases the reflective properties of pure magnetite, hence less neutrons return to the fuel.

Another case with the magnetite layer replaced by water (in case Fe(II) ions are mainly sorbed or involved in clay transformations, as iron corrosion studies in the presence of clay indicate) was also analysed. The reactivity of the insert with a magnetite layer corresponding to the corrosion of a relatively small amount (2 mm) of carbon steel present and absent (Fe(II) ions assumed to sorbed by clay) is compared in Table 6-2.

Table 6-2. Calculated k_{eff} for the corrosion of 2 mm steel with the magnetite present compared to the case when the layer of magnetite is replaced by water.

Insert type	Magnetite present	Magnetite replaced by water	Δk_{eff}
BWR P355N	0.95857	0.94118	−0.01739
PWR P355N	0.91103	0.90540	−0.00563
BWR P460N	0.93263	0.91480	−0.01783
PWR P460N	0.91129	0.90654	−0.00475

The conclusion is like that in (Agrenius and Spahiu 2016) that the reactivity will be lower in this case, as compared to the case with magnetite remaining in the gap between framework plates and the fuel assembly, since magnetite is a better neutron reflector than water.

Hydrogen is produced during the corrosion process. The effect of dissolved hydrogen in the water was investigated.

About 40 mM hydrogen could be dissolved in water at 50 bars pressure. Calculations show that this hydrogen concentration will have some, although small, effect on the reactivity:

Insert material P355N: $\Delta k_{eff} = 0.00007$ for PWR and $\Delta k_{eff} = 0.00004$ for BWR

Insert material P460N: $\Delta k_{eff} = 0.00027$ for PWR and $\Delta k_{eff} = -0.00019$ for BWR.

The influence of dissolved hydrogen is at the detection limit for the P355N insert, and slightly more pronounced for the P460N insert.

6.4.2 Other anoxic corrosion products

Besides magnetite, siderite ($FeCO_3$) or mackinawite (FeS) could form in the canister. This was discussed in Section 6.3, while in the Appendix C the calculations of the composition of the siderite + magnetite and mackinawite + magnetite mixtures have been carried out separately for the PWR and BWR cases, both for P355N and P460N inserts. The calculation concerns the case when the mixed corrosion product layer almost touches the fuel rods in the PWR case and the case when all the space outside the fuel channels is filled with corrosion products in the BWR case, but there is water between the fuel rods.

As discussed in Section 6.3, a maximum of 1.8 moles siderite per year could be produced in each canister based on the groundwater composition in Forsmark. In the same way, assuming all sulphate converted to sulphide by SRB bacteria a maximum of 1.5 moles mackinawite per canister and year could be formed. The calculation is slightly different for the PWR and BWR insert which have different surface areas of steel corroding. The total amount of iron corroded per year with a corrosion rate 1 µm/year is different for a PWR canister (~27.7 or 39 m^2) and a BWR canister (~53.4 or 57.6 m^2).

The results are shown in Table 6-4 and Table 6-5 for the PWR P355N and PWR P460N cases respectively. As seen from the tables, mixtures of magnetite with siderite give a slightly higher reactivity compared with the case with pure magnetite for the PWR inserts, while mixtures of magnetite with mackinawite give slightly lower reactivities than pure magnetite in all cases.

Table 6-3. Calculated cases with mixtures of magnetite and siderite ($FeCO_3$), respectively mackinawite (FeS), for the PWR P355N insert.

Mixture	Density of mixture (g/cm^3)	P-B ratio	k_{eff}	Δk compared to main case
100 % Fe_3O_4 (main case)	5.17	2.1	0.91289	-
43.7 % Fe_3O_4 + 56.3 % $FeCO_3$	4.35	3.07	0.91364	0.00075
59 % Fe_3O_4 + 41 % $FeCO_3$	4.54	2.77	0.91335	0.00046
58.3 % Fe_3O_4 + 40.7 % FeS	4.78	2.35	0.90704	−0.00585
70.3 % Fe_3O_4 + 29.7 % FeS	4.88	2.28	0.90850	−0.00439

Table 6-4. Calculated cases with mixtures of magnetite and siderite ($FeCO_3$), respectively mackinawite (FeS), for PWR P460N.

Mixture	Density of mixture (g/cm^3)	P-B ratio	k_{eff}	Δk compared to main case
100 % Fe_3O_4 (main case)	5.17	2.1	0.91092	-
57.7 % Fe_3O_4 + 42.3 % $FeCO_3$	4.53	2.79	0.91219	0.00127
66.5 % Fe_3O_4 + 33.5 % $FeCO_3$	4.59	2.62	0.91190	0.00098
70.8 % Fe_3O_4 + 29.2 % FeS	4.88	2.28	0.90660	−0.00432
77 % Fe_3O_4 + 23 % FeS	4.94	2.24	0.90565	−0.00527

The calculations for the BWR canister are done for the case when all the space outside the fuel channels is filled with corrosion product mixtures, but there is water between fuel rods and are shown in Table 6-5 for BWR P355N and in Table 6-6 for BWR P460N. Even here mixtures of magnetite with mackinawite give lower reactivity then pure magnetite, while mixtures of siderite with magnetite give higher reactivity than pure magnetite for BWR P460N insert, but a slightly lower reactivity than pure magnetite for the BWR P355N insert.

Table 6-5. Calculated cases with mixtures of magnetite plus siderite ($FeCO_3$), and magnetite plus mackinawite (FeS), for the BWR P355N insert.

Mixture	Density of mixture (g/cc)	P-B ratio	k_{eff}	Δk compared to main case
100 % Fe_3O_4 (main case)	5.17	2.1	0.98178	-
67.9 % Fe_3O_4 + 32.1 % $FeCO_3$	4.67	2.60	0.98150	−0.00028
73.5 % Fe_3O_4 + 26.5 % $FeCO_3$	4.75	2.51	0.98155	−0.00023
78.5 % Fe_3O_4 + 21.5 % FeS	4.95	2.23	0.97544	−0.00634
82 % Fe_3O_4 + 18 % FeS	4.99	2.21	0.97633	−0.00545

Table 6-6. Calculated cases with mixtures of magnetite plus siderite ($FeCO_3$), and magnetite plus mackinawite (FeS), for the BWR P460N.

Mixture	Density of mixture (g/cc)	P-B ratio	k_{eff}	Δk compared to main case
100 % Fe_3O_4 (main case)	5.17	2.1	0.96452	-
70 % Fe_3O_4 + 30 % $FeCO_3$	4.70	2.57	0.96533	0.00081
75 % Fe_3O_4 + 25 % $FeCO_3$	4.77	2.48	0.96503	0.00051
80 % Fe_3O_4 + 20 % FeS	4.97	2.22	0.95810	−0.00642
83.1 % Fe_3O_4 + 16.9 % FeS	5.00	2.20	0.95802	−0.00650

6.4.3 Magnetite falls down into the channels of the canister

As discussed in Section 6.3, it is difficult to predict the behaviour of the corrosion layer for such large time spans and expert judgement was used to assume that all the magnetite will stick to the framework plates or the load bearing tube. In this section a case is analysed assuming that the magnetite will fall into the channel in a PWR canister. In this case it is assumed that the magnetite layer which touches the fuel rods will fall down into the lower part of the fuel assembly. The result is that the space between fuel rods in the bottom part of the fuel assembly will be filled by magnetite and the top part will be surrounded by a larger water gap. The result is $k_{eff} \pm \sigma = 0.89363$. This calculation is done with crystalline magnetite. The reduction of the reactivity is $\Delta k = 0.01729$ compared to the maximum reactivity case, discussed in Section 6.4.1.

A similar calculation for the most reactive configuration of the PWR P460N insert if the formed magnetite falls down and fills the lower 2.76 m of the insert gives $k_{eff} = 0.89262$, corresponding to a reduction of reactivity $\Delta k = 0.0183$ as compared to the case when magnetite sticks to the corroding surfaces assumed in the base case in 6.4.1.

In the BWR case with fuel channels (Zircaloy box), the walls of the fuel channel will prevent the magnetite from falling into the fuel assembly, so only the magnetite above the fuel channel may fall into the fuel assembly. In the case of Concept 1 inserts it was assumed that this magnetite contributes to the filling of all the free space outside the fuel channels, because this gives more reactive configurations; hence no calculations with magnetite falling down were carried out for the BWR inserts.

6.4.4 Magnetite layer grows resulting in reduced fuel rod pitch

In spite of the arguments presented for the mechanical properties of the hydrated magnetite, a calculation case with the expanding magnetite layer assumed to be stiff and exert pressure on the fuel assembly pushing the fuel rods closer to each other was carried out. In these cases, it is assumed that the pitch is reduced 0.3 mm both in the PWR case and the BWR case. The results are shown below for the P355N inserts:

BWR: $k_{eff} = 0.97922$, $\Delta k_{eff} = -0.00173$ compared to the max reactivity ($k_{eff} = 0.98178$)

PWR: $k_{eff} = 0.91200$, $\Delta k_{eff} = -0.00089$ compared to the max reactivity case in 6.4.1.

and for the P460N inserts:

BWR: $k_{eff} = 0.96276$, $\Delta k_{eff} = -0.00176$ compared to the max reactivity case in 6.4.1

PWR: $k_{eff} = 0.91076$, $\Delta k_{eff} = -0.00016$ compared to the max reactivity case in 6.4.1.

The explanation of this reactivity behaviour is due to that the fuel lattice is designed to have a fuel/moderator ratio close to the optimal, but slightly under-moderated, to enable negative temperature reactivity feedback. If you increase the fuel/moderator ratio the reactivity will decrease.

6.4.5 Magnetite extrudes into the fuel assembly

The next situation analysed here after the one when the corrosion product layer contacts the fuel rods in the PWR insert or fills all the space outside the 12 fuel channels in the BWR insert, is the case when the whole free space in the insert, including that between fuel rods, is filled with corrosion products as the corrosion continues. This will be achieved at different times for the PWR and BWR inserts, since they have different free volumes and internal surface areas.

For the PWR P355N insert the internal surface area is 27.71 m^2 while the total free volume of a loaded canister is 1.244 m^3 (Table 5-3). The volume of iron (denoted X) needed to corrode to fill all the free space with crystalline magnetite ($R_{P\text{-}B} = 2.1$) is found from $2.1 \times X = X + 1.244$, which gives X = 1.131 m^3 iron. This produces 2.375 m^3 magnetite, which fills all the initial free volume (1.244 m^3) plus the volume of corroded iron (1.131 m^3). The lid and base plates are 56 mm thick and after 28 000 y are completely corroded. At this point in time, the amount of iron corroded is 27.71 $m^2 \times 0.028$ m = 0.776 m^3. The remaining 0.355 m^3 iron will corrode from a smaller surface (this of the framework plus the inner surface of thick tube) of 26.76 m^2. Continued corrosion of this reduced surface with 13.3 mm (41.3 mm in total) accomplishes the filling of all the free space with crystalline magnetite. At this point in time, i.e., after 41 300-year corrosion with 1 µm/y producing crystalline magnetite the whole space inside the insert is filled with magnetite. The thick loadbearing tube has 4.9 mm steel uncorroded while the framework plates have 3.4 mm steel uncorroded. This situation of the canister is presented in Figure 6-7 and the calculated k_{eff} is 0.37385.

For the BWR P355N canister the internal surface area is 53.39 m^2 while the total void volume in a loaded canister is 0.972 m^3. The volume of iron needed to corrode to fill all the free space in canister with magnetite is found from $2.1 \times X = X + 0.972$ and results in 0.884 m^3 iron. This means that after 16.55 mm corrosion of the internal surface all the free space including that between fuel rods is filled with magnetite. In fact, after 16 mm corrosion from both sides the 32 mm steel plates are completely corroded. At this point in time about 97 % of the free space in the canister is filled with magnetite and the remaining 3 % iron will corrode from a smaller surface consisting of the thick corner beams and the steel tube plus top and bottom plates of a total surface 22.99 m^2, causing an additional 1.3 mm corrosion in the remaining surface. This situation of the canister is presented in Figure 6-8 with 32 mm steel plates corroded completely and 17.3 mm steel corrosion of the load bearing tube, corner beams as well as from the lead and base plates. The reactivity of the canister decreases very much when corrosion products replace the water between the fuel rods, $k_{eff} = 0.38953$.

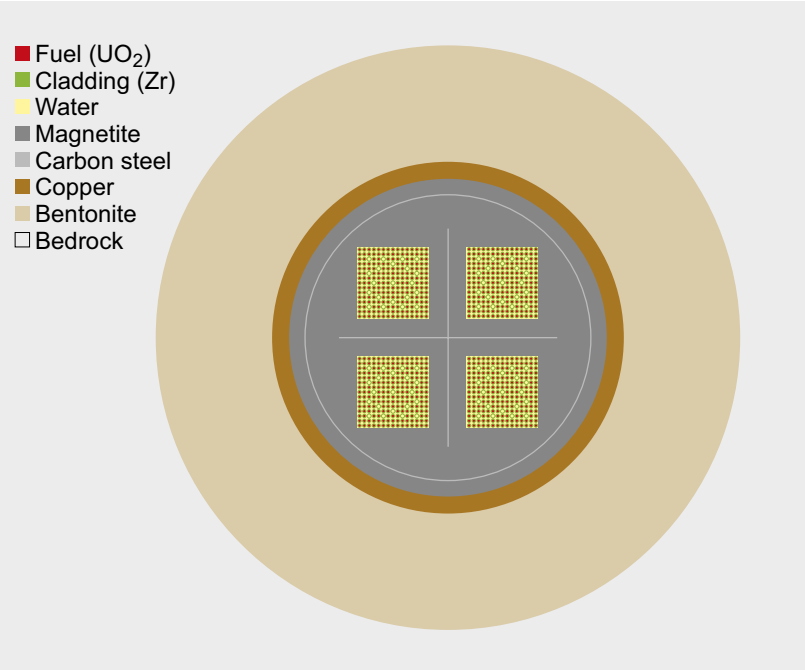

Figure 6-7. *Cross section of PWR P355N canister after 41 300 y corrosion.*

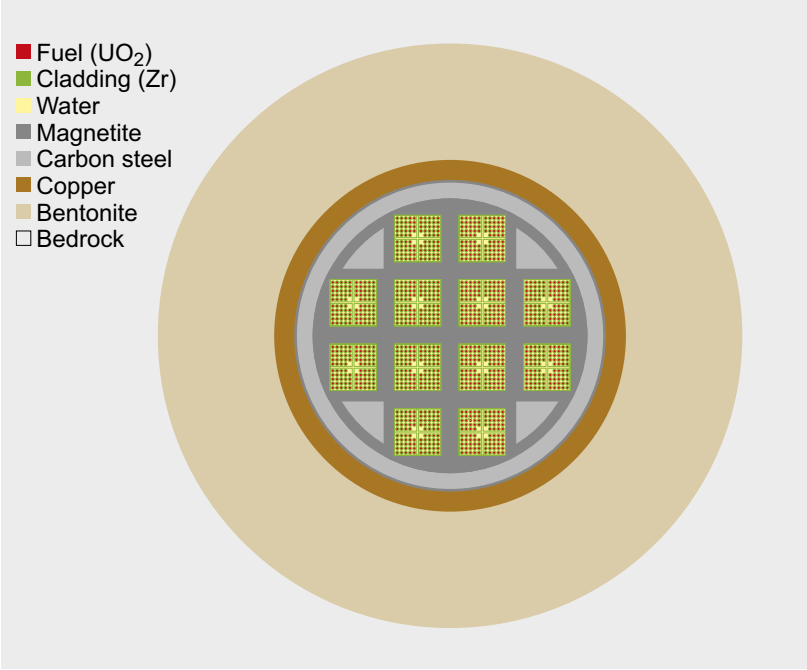

Figure 6-8. *Cross section of BWR P355N canister after ~17 300 y corrosion.*

In a loaded PWR P460N canister the free volume is 0.988 m^3 while the internal corroding surface is 39.07 m^2 (Table 5-3). The free space in the insert including this between fuel rods will be completely filled with crystalline magnetite when 0.898 m^3 iron has corroded. This corresponds to the corrosion of 0.898 m^3/39.07 m^2 = 0.02299 m or 23 mm steel from all the internal surfaces. The situation in this insert after 23 000 y corrosion is presented in Figure 6-9. The reactivity of the canister decreases when magnetite substitutes water between the fuel rods, k_{eff} = 0.34852.

Finally, for the BWR P460N insert, the free volume in the loaded insert is 1.072 m^3 while the internal surface area is 57.58 m^2 (Table 5-3). All the free space in the insert including this between fuel rods will be filled with magnetite when a volume X of iron has corroded, which is found from the relationship $2.1 \times X = X + 1.072$, which gives X = 0.975 m^3 iron. This situation in the canister is realized after the corrosion of 0.975 m^3/57.58 m^2 = 0.0169 m or 16.9 mm steel and is shown in Figure 6-10. The reactivity decreases, as in the other cases with magnetite between the fuel rods, k_{eff} = 0.37345.

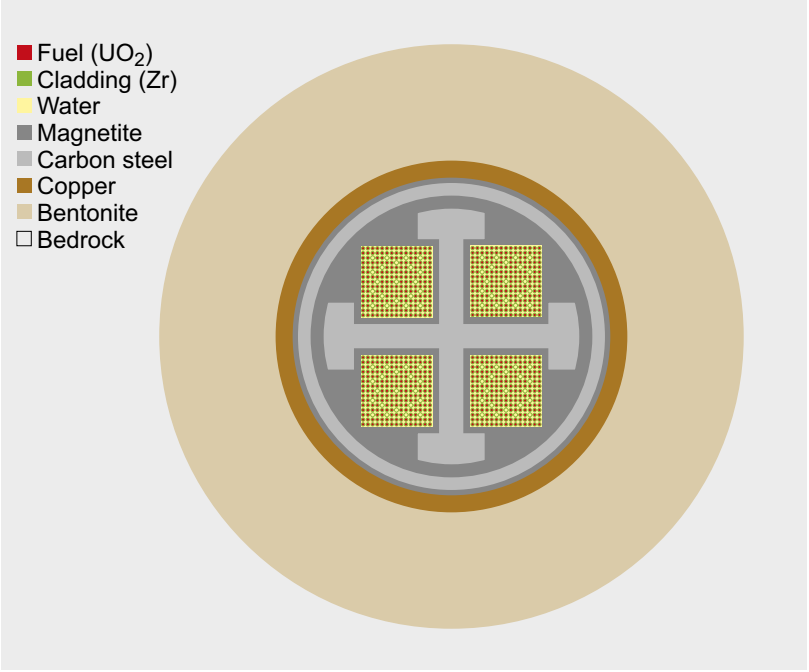

Figure 6-9. *Cross section of a PWR P460N canister after 23 000 y corrosion.*

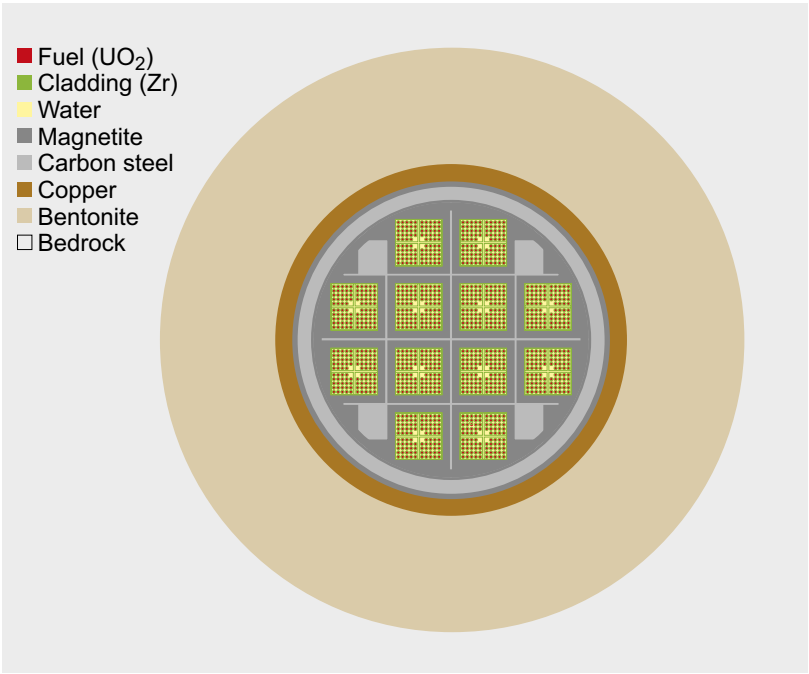

Figure 6-10. *Cross section of a BWR P460N canister after 16 900 y corrosion.*

The reactivities of the above canister configurations with all the free space filled with magnetite were calculated also for hydrated magnetite with different water contents. The results are shown in Figure 6-11 for the P355N inserts and in Figure 6-12 for the P460N steel grade inserts.

As seen in Figure 6-11 and Figure 6-12 the reactivity of the corrosion product filled insert increases with the water content in magnetite, but is always lower than that for the base case (magnetite layer touches fuel rods for PWR insert or all the free space outside the fuel channels filled with crystalline magnetite for BWR insert) discussed in 6.4.1. The explanation to this reactivity behaviour is that the moderation inside the fuel lattice will be better when increasing the water content in the magnetite.

During the review of this report, it was pointed out that such large water contents in hydrated magnetite correspond to unreasonably high porosities. This means that especially the data for 20 wt% and 30 wt% water should be disregarded.

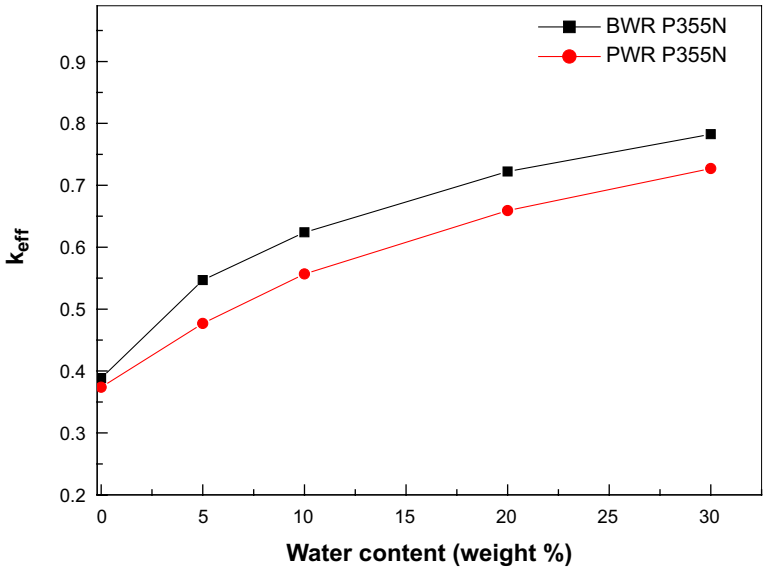

Figure 6-11. *Variation of k_{eff} in a canister where all the free space is filled with hydrated magnetite containing various amounts of water for the P355N inserts.*

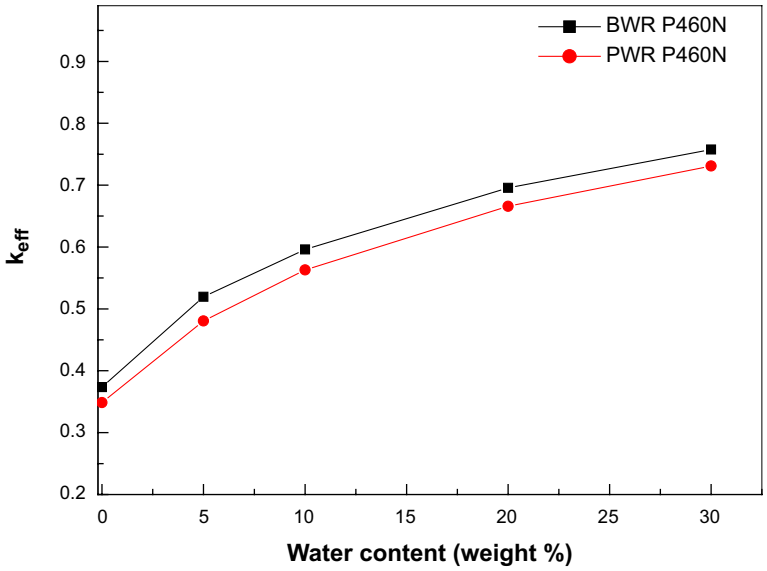

Figure 6-12. *Variation of k_{eff} in a canister filled with hydrated magnetite as a function of the water content for the P460N inserts.*

A final case concerns the complete corrosion of the framework plates and the load bearing tube in the 4 insert variants discussed here. This will occur at different times and was simulated by calculating the whole insert filled with magnetite including the space between the fuel rods, neglecting any metallic part which has not corroded completely and assuming the copper shell has not deformed. The reactivities for the P355N insert were:

BWR: $k_{eff} = 0.39695$

PWR: $k_{eff} = 0.37385$

In the case of the P460N insert the results are:

BWR: $k_{eff} = 0.37345$

PWR: $k_{eff} = 0.34852$

After all the free space in the canister has been filled with carbon steel corrosion products, it seems difficult to envisage major changes in the geometry of the damaged canister, unless the copper shell is deformed. Further steel corrosion after all the free space has been filled with magnetite will cause some compaction of the corrosion product, but the excess magnetite is expected to be pressed out of the canister at the defect in the shear load scenario or the corroded Cu region in the erosion-corrosion scenario. Alternatively, an expansion of the copper shell is possible. In this report no calculation of the expansion of the copper shell by corrosion products was made because a similar calculation for the reference insert indicated that very small increases in reactivity as compared to the undeformed copper shell were obtained, all with low reactivities, quite comparable to that of the insert filled with corrosion products.

6.4.6 Zirconium in the cladding and BWR fuel channel converted to zirconium oxide

In Section 6.3.3 it was argued that Zircaloy corrodes much slower than other materials and despite the limited thickness of cladding, it may not have corroded completely when the insert is filled with magnetite. In this section a calculation case is considered in which Zircaloy corrodes faster so that it is completely converted to zirconium oxide when the insert reaches the most reactive configuration. The following cases were calculated:

For the PWR P355N and P460N inserts, all zircaloy in the cladding is converted to zirconium oxide just when the magnetite layer touches the fuel rods, but the fuel column[13] is intact, that is the full corrosion of cladding coincides with the achievement of the most reactive configuration. The results are:

$k_{eff} = 0.89443$ for PWR P355N and $k_{eff} = 0.89527$ for PWR P460N

For the BWR inserts the following situation is modelled: zirconium oxide replaces zirconium in the cladding and the corresponding part of the fuel channel material, the fuel column is still intact when all the space outside the 12 fuel channels is filled with magnetite. The results are:

$k_{eff} = 0.95758$ for BWR P355N and $k_{eff} = 0.93563$ for BWR P460N

In all cases, k_{eff} is lower than in the main case discussed in Section 6.4.1. This is due to the volume increase during zircaloy corrosion ($R_{P\text{-}B} = 1.56$ for ZrO_2) which reduces the water content in the fuel and consequently the reactivity.

6.4.7 Radial movement of fuel rods

Movement of part length rods could happen if spacers are consumed by corrosion. In Section 6.4.7 of (Agrenius and Spahiu 2016) the reactivity effect of moving part length rods was investigated for SVEA-96 Optima 3 as they are most likely to move because they have the least number of attachments to the structural parts of the fuel assembly. The results show that moving the part length rods inside the fuel channel can result in a reactivity increase with up to 0.0034 ($\Delta k_{eff} = 0.0034$). It is considered very

[13] The fuel column is the stack of uranium pellets within the cladding.

unlikely that this will create a more reactive configuration than the initial case with evenly distributed spaces between fuel rods by chance. This general conclusion is also valid for other fuel types. If a higher reactivity configuration should be likely to occur when the spacers are corroded, there must be a driving force that evenly expands the fuel lattice. This is not foreseen and therefore this case is not considered further in this report, and should be seen as a "what if" scenario.

It should also be noted that those calculations were carried out for an uncorroded canister, which is not realistic. Even the thinnest grid spacers (0.3 mm, SKB 2022b), made of corrosion resistant Inconel or Zircaloy, would corrode completely from both sides after 15 000 years with a corrosion rate of 0.01 μm/year, while with the recently reported corrosion rates for SS 304 by Sakuragi (2017), they would corrode completely from both sides after 375 000 years (3×10^{-4} m/2 × 4×10^{-10} m/year = 3.75×10^{5} years). The BWR inserts discussed here are filled with magnetite between the fuel rods in less than 17 300 years, i.e., much before than the expected grid spacer complete corrosion occurs with the recent corrosion rates.

6.4.8 Fuel pellets fall down to the bottom of the canister

According to the analysis carried out for the reference insert (Section 6.4.8 in Agrenius and Spahiu 2016) the reactivity decreases when the UO_2/water ratio increases, i.e., when there is more UO_2 per volume of water. This occurs when pellets fall down in the channel to the bottom of the canister. The four insert types discussed here are not symmetrical as is the reference insert and the free volumes are not equal in the different compartments, which makes the calculation more complex. In any case, the conclusion that the reactivity decreases when the UO_2/water ratio increases also holds in this case and for this reason this case was not investigated further here.

6.4.9 Corrosion of UO_2

The fuel cladding is not considered as a barrier to water in the safety assessment, hence when the corrosion of all the materials in a breached canister starts, it includes the corrosion/oxidative dissolution of spent nuclear fuel too. The oxidative dissolution of the UO_2 fuel matrix is caused by radiolytic oxidants and consists in the release of some U(VI) from the fuel, which is later reduced and precipitated as UO_2(s) on the surface of the corroding iron.

The calculations were carried out with fresh fuel as in the other cases and the lowest corrosion rate of carbon steel (0.1 μm/y) was considered, since this gives higher amounts of fissile material deposited on the surface of the corroding iron.

In the case of the BWR inserts discussed in this report, the magnetite formed e.g., in the central channels of the insert is assumed to contribute to the filling of the free space in the peripheral channels, which have higher free volume, until all the space outside the 12 fuel channels (BWR Zicaloy boxes) is filled with magnetite. In this case the uranium released during the years required to fill all the space outside the fuel channels with magnetite for a corrosion rate 0.1 μm/y was assumed to be mixed homogeneously in the magnetite layer, since this mixing is reasonable to assume during the magnetite transport to peripheral compartments. The calculated reactivity of the BWR P355N insert considering precipitated UO_2 mixed in the magnetite for the most reactive configuration (the whole space outside the fuel channels filled with magnetite, but water between fuel rods) resulted in $k_{eff} = 0.97863$, i.e., a decrease by $\Delta k_{eff} = -0.00315$ compared to the most reactive case. A similar calculation for BWR P460N resulted in $k_{eff} = 0.96016$, a decrease by $\Delta k_{eff} = -0.00435$ compared to the most reactive configuration discussed in Section 6.4.1. The decrease is due to the fact that fuel mixed in the magnetite lacks the moderation that water provides and is therefore not contributing much to reactivity.

For the PWR case such mixing does not exist, and the re-deposited fissile material was modelled on the surface of the magnetite layer. This resulted in a very slight increase in reactivity for the PWR P355N insert, $k_{eff} = 0.91295$ and $\Delta k_{eff} = 0.00006$. The calculations for the PWR P460N insert with a layer of fissile material deposited on the surface of the magnetite resulted in $k_{eff} = 0.91062$, and $\Delta k_{eff} = -0.00030$, i.e., a in decrease of reactivity by 30 pcm as compared to the most reactive configuration.

In (Agrenius and Spahiu 2016) the reactivity increase for the case with re-deposited material was larger. However, in that case there was another insert geometry, cast iron insert, where all the fissile material was redeposited on the insert walls, i.e., on the surfaces closest to the fuel rods. In the current geometry parts of the material will be deposited on the free surfaces at a certain distance from the fuel rods and hence contribute less to the reactivity increase. Another aspect is that the calculations in (Agrenius and Spahiu 2016) were performed with 3.5 % HM, U + Pu (2.6 % + 0.9 %). This is more than the requirements for burn-up credit will allow and does not consider that Pu-239 will partly decay during the relatively long time it takes to fill the insert with magnetite.

6.5 Analysis

The reactivity development is summarized in Table 6-7 and Table 6-8 for P355N and P460N inserts, respectively. The cases are assigned numbers in order to facilitate the analysis and comparison between the different cases.

Table 6-7. Summary of the calculated cases for the P355N inserts.

Case no	Description	BWR P355N		PWR P355N	
		k_{eff}	Δk compared to base case	k_{eff}	Δk compared to base case
1	Dry canister	0.21328		0.16424	
2	Base case, water-filled canister, no corrosion	0.94695		0.90772	
3	Crystalline magnetite in gap or all space outside fuel channels	**0.98178**	**0.03483**	0.91289	0.00517
4	Hydrated magnetite – 5 % water (gap/outside fuel channels)	0.95759	0.01064	0.90488	−0.00801
5	Hydrated magnetite – 10 % water (gap/outside fuel channels)	0.94868	0.00173	0.90299	−0.00473
6	Hydrated magnetite – 20 % water (gap/outside fuel channels)	0.94263	−0.00432	0.90249	−0.00523
7	Hydrated magnetite – 30 % water (gap/outside fuel channels)	0.94087	−0.00608	0.90315	−0.00457
8	2 mm corrosion, magnetite replaced by water	0.94118	−0.00577	0.90540	−0.00232
9	$FeCO_3$ + Fe_3O_4 in gap	0.98155	0.03460	**0.91364**	**0.00592**
10	FeS + Fe_3O_4 in gap	0.97633	0.02938	0.90849	0.00077
11	Magnetite layer (5.17 g/cm^3) falls down into fuel	-	-	0.89363	−0.01409
12	Reduced rod pitch, magnetite fills gap or space outside fuel channels.	0.98005	0.03310	0.91200	0.00428
13	Magnetite flows into fuel (5.17 g/cm^3)	0.38953	−0.55742	0.37385	−0.53387
14	Hydrated magnetite (5 % water) flows into fuel	0.54833	−0.39862	0.47674	−0.43098
15	Hydrated magnetite (10 % water) flows into fuel	0.62435	−0.3226	0.55681	−0.35091
16	Hydrated magnetite (20 % water) flows into fuel	0.72205	−0.2249	0.65905	−0.24867
17	Hydrated magnetite (30 % water) flows into fuel	0.78204	−0.16491	0.72700	−0.18072
18	The whole insert is corroded	0.39695	−0.55000	0.37502	−0.5327
19	Magnetite 5.17 g/cm^3, Zr oxidized, fuel column intact	0.95758	0.01063	0.90276	−0.00446

Table 6-8. Summary of the calculated cases for the P460N inserts.

Case no	Description	BWR P460N		PWR P460N	
		k_{eff}	Δk compared to base case	k_{eff}	Δk compared to base case
1	Dry canister	0.20547		0.16565	
2	Water-filled canister, no corrosion	0.92134		0.90778	
3	Crystalline magnetite in gap or outside fuel channels	0.96452	0.04318	0.91092	0.00314
4	Hydrated magnetite – 5 % water	0.93336	0.01202	0.90274	−0.00504
5	Hydrated magnetite – 10 % water	0.92366	0.00226	0.90096	−0.00682
6	Hydrated magnetite in gap – 20 % water	0.91730	−0.00404	0.90017	−0.00761
7	Hydrated magnetite in gap – 30 % water	0.91649	−0.00485	0.90107	−0.00593
8	Magnetite replaced by water for 2 mm corrosion	0.91480	−0.00654	0.90654	−0.00124
9	$FeCO_3$ + Fe_3O_4 in gap or space outside fuel channels	**0.96533**	**0.04399**	**0.91219**	**0.00441**
10	FeS + Fe_3O_4 in gap or space outside fuel channels	0.95902	0.03768	0.90660	−0.00118
11	Magnetite layer falls down into PWR fuel	-		0.89262	−0.01516
12	Reduced rod pitch (gap closed/space outside fuel channels filled)	0.96276	0.04142	0.91076	0.00298
13	Magnetite flows into fuel 5.17 g/cm^3	0.37345	−0.54789	0.34852	−0.55926
14	Hydrated magnetite (5 % water) flows into fuel	0.51950	−0.40184	0.48046	−0.42732
15	Hydrated magnetite (10 % water) flows into fuel	0.59604	−0.3252	0.56299	−0.34479
16	Hydrated magnetite (20 % water) flows into fuel	0.69562	−0.22572	0.66581	−0.24187
17	Hydrated magnetite (30 % water) flows into fuel	0.75774	−0.16360	0.73088	−0.17690
18	The whole insert is corroded	0.38039	−0.54095	0.36263	−0.54515
19	Magnetite 5.17 g/cm^3, Zr oxidized, fuel column intact	0.93563	0.01429	0.89527	−0.01251

7 Summary and conclusions

Assuming that disposal canisters are water-filled, the corrosion of the carbon steel insert will generate corrosion products. These have lower density than iron so the water gap between the fuel assemblies and the framework will close. Further, in the BWR insert a more reactive configuration is realized when all the space outside the fuel channels (Zircaloy boxes) is filled with corrosion products while there is still water inside the fuel channels.

If the corrosion product is crystalline magnetite this effect will increase the reactivity with $\Delta k_{eff} = 0.03483$ for BWR P355N and $\Delta k_{eff} = 0.00517$ for PWR P355N inserts compared to the base case (case 2 in Table 6-7). Assuming that siderite is also produced besides magnetite, the reactivity will increase further for the PWR P355N insert by $\Delta k_{eff} = 0.00075$(case 9 versus case 3). Instead, a decrease in presence of siderite as compared to pure magnetite is noted for the BWR P355N insert. Considering the hydrogen that will be dissolved in the groundwater, an additional reactivity increase will occur, $\Delta k_{eff} = 0.00007$ for PWR and $\Delta k_{eff} = 0.00004$ for BWR for a concentration of 40 mM dissolved hydrogen (Section 6.4.1). Corrosion of the fuel can result in the release of oxidized U species, which are afterwards reduced and precipitated on the corroded iron layer. This will give additional reactivity increase for PWR P355N by $\Delta k_{eff} = 0.00006$ while for BWR P355N insert a slight decrease is observed (Section 6.4.9). The radial movement of the part length fuel rods is considered as a "what if" scenario and is not included in the summary.

Table 7-1. Summary of reactivity effects for the P355N inserts.

Effect	Reactivity increase Δk	
	BWR	PWR
Gap or space outside fuel channels filled with magnetite	0.03483	0.00517
Magnetite + siderite in gap/space outside fuel channels	-	0.00075
H_2 dissolved in water	0.00004	0.00007
UO_2 on magnetite surface (PWR)	-	0.00006
Sum	0.03487	0.00605

When the corrosion product is crystalline magnetite, filling of the gap or the space outside the fuel channels will increase the reactivity with $\Delta k_{eff} = 0.04318$ for BWR P460N and $\Delta k_{eff} = 0.00414$ for PWR P460N compared to the base case (case 2 in Table 6-8). Assuming that siderite is also produced besides magnetite, the reactivity will increase further by $\Delta k_{eff} = 0.00081$ for the PWR P355N insert and $\Delta k_{eff} = 0.00127$ for the BWR P460N insert (case 9 versus case 3 in Table 6-8). Considering the 40 mM hydrogen that will be dissolved in the groundwater, an additional reactivity increase occurs for the PWR P460N insert with $\Delta k_{eff} = 0.00027$, and a reactivity decrease occurs for the BWR P460N insert with $\Delta k_{eff} = -0.00019$, (Section 6.4.1). Corrosion of the fuel results in the release of oxidized U species, which are afterwards reduced and precipitated on the corroded iron layer. This results in a reactivity decrease for PWR P460N by $\Delta k_{eff} = -0.00030$ while for BWR P460N insert the decrease is larger $\Delta k_{eff} = -0.00435$ (Section 6.4.9). The effects on reactivity are summarized in Table 7-2.

Table 7-2. Summary of reactivity effects for the P460N inserts.

Effect	Reactivity increase Δk	
	BWR	PWR
Gap or space outside fuel channels filled with magnetite	0.04318	0.00314
Magnetite + siderite in gap/space outside channels	0.00081	0.00127
H_2 dissolved in water	−0.00019	0.00027
UO_2 on magnetite surface (PWR)	−0.00435	−0.00030
Sum	0.03945	0.00438

In summary it is shown here that the reactivity in the Rebus Concept 1 insert can be held at levels that meets the criteria including the effects on reactivity from corrosion. The analysis includes assumptions on burnup and burnable poison that implies use of credit for burnup for the PWR case and poison for BWR. The reactivity for the BWR P355N insert is higher than for the cast iron (reference) insert whereas the reactivity is lower for the PWR P355N insert. The increase in reactivity for the BWR P355N insert is limited and can be handled with analytical measures, for example burnup credit. For PWR the required burnup will be less than for the reference insert. The final requirement on burnup, or other possible measures of reactivity control, will be settled in the criticality analysis for the final repository.

References

SKB's (Svensk Kärnbränslehantering AB) publications can be found at www.skb.com/publications. SKBdoc documents will be submitted upon request to document@skb.se.

ACI, 2007. ACI Manual of Concrete Inspection. 10th edition. Farmington Hills: American Concrete Institute.

Agrenius L, Spahiu K, 2016. Criticality effects of long-term changes in the material compositions and geometry in disposal canisters. SKB TR-16-06, Svensk Kärnbränslehantering.

Baldwin, T D, Mason R, Hicks T W, 2016. Types of critical systems and the credibility of rapid transient criticality in a geological disposal facility. Galson Science ltd, Report No. 1541-1, Radioactive Waste Management, United Kingdom.

Blackwood D J, Naish C C, Sharland S M, Thompson A M, 2002. Experimental and modelling study to assess the initiation of crevice corrosion in stainless steel containers for radioactive waste. Report AEAT/ERRA-0300, AEAT Technology, United Kingdom.

CRC, 2012. CRC Handbook of chemistry and physics. 93rd ed. Boca Raton: CRC Press.

Cui D, Spahiu K, 2002. The reduction of U(VI) on corroded iron under anoxic groundwater conditions. Radiochimica Acta 90, 1–6.

Dinh H T, Kuever J, Mussmann M, Hassel A W, Stratmann M, Widdel F, 2004. Iron corrosion by novel anaerobic microorganisms. Nature 427, 829–832.

Diomidis N, 2014. Scientific basis for the production of gas due to corrosion in a deep geological repository. NAB 14-21, National Cooperative for the Disposal of Radioactive Waste, Switzerland.

Enning D, Garrelfs J, 2014. Corrosion of iron by sulphate-reducing bacteria: New views on an old problem. Applied Environmental Microbiology 80, 1226–1236.

Feron D, Cruset D, Gras J-M, 2009. Corrosion issues in the French high-level nuclear waste programme. Corrosion 65, 213–223.

Fiedor J N, Bostick W D, Jarabek R, Farrell J, 1998. Understanding the mechanism of uranium removal from groundwater by Zero Valent Iron using X-ray photoelectron spectroscopy. Environmental Science & Technology 32, 1466–1473.

Farrell J, Bostick W D, Jarabek R, Fiedor N, 1999. Uranium removal from ground water using zero valent iron media. Groundwater 37, 618–624.

Grambow B, Smailos E, Geckeis H, Müller R, Hentschel H, 1996. Sorption and reduction of uranium (VI) on iron corrosion products under reducing saline conditions. Radiochimica Acta 74, 149–154.

Gras J-M, 2014. State of the art of 14C in Zircaloy and Zr alloys-14C release from zirconium alloy hulls. Deliverable 3.1 of the EU-Project Cast. CAST-2014-D.3.1, L'Agence nationale pour la gestion des déchets radioactifs, France.

Gu B, Liang L, Dickey J, Dai S, 1998. Reductive precipitation of uranium (VI) by zero-valent iron. Journal of Environmental Science and Technology 32, 3366–3373.

Hansson N I, Saleh M, Tam E, Holgerson S, Spahiu K, Ekberg C, 2023. Influence of groundwater composition on the reductive precipitation of U(VI) on corroding iron surfaces. Journal of Nuclear Materials 577, 154324.

Hedin A, Zetterström-Evins L, Spahiu K, 2013. What if criticality in a final repository. SKBdoc 1417199 ver 1.0, Svensk Kärnbränslehantering AB.

Hicks, T W, Doudou S, Baldwin T D, 2017. The likelihood of criticality and the credibility of rapid transient criticality following geological disposal of MOX, new build, metallic and exotic spent fuel. Report 1587-2, Galson Sciences Ltd, United Kingdom.

Hicks, T W, Doudou S, Walters, W S 2018. Demonstrating the criticality safety of the spent fuel disposal. RWM GLS-1649-5-V3.1, Radioactive Waste Management, United Kingdom.

IAEA, 2006. Understanding and managing ageing of materials in spent fuel storage facilities. IAEA Technical Reports Series No. 443, International Atomic Energy Agency, Austria.

Jelinek J, Neufeld P, 1982. Kinetics of hydrogen formation from mild steel in water under anaerobic conditions. Corrosion 38, 98–104.

Johnson A B, Burke S P, 1996. K-Basin Corrosion Report. WHC-EP-087, Westinghouse Hanford Company, USA.

Jonsson M, Emilsson G, Emilsson L, 2018. Mechanical design analysis for the canister. Posiva SKB Report 04, Posiva Oy, Svensk Kärnbränslehantering AB.

Joyce S, Woollard A, Marsic N, Sidborn M, 2015. Future evolution of groundwater composition at Forsmark during an extended temperate period. SKB R-14-26, Svensk Kärnbränslehantering AB.

King F, 2008. Corrosion of carbon steel under anaerobic conditions in a repository for SF and HLW in Opalinus Clay. Nagra Technical Report 08-12, National Cooperative for the Disposal of Radioactive Waste, Switzerland.

King F, 2014. Durability of high level waste and spent fuel disposal canisters-an overview of the combined effect of chemical and mechanical degradation mechanisms. Appendix B2: Corrosion of carbon steel. RWMD Report 17697/TR/03, Radioactive Waste Management, United Kingdom.

King F, Burt D, Ganeshalingam J, Gardner P, Sanderson D, Watson S, Padovani C, 2014. Coupled analysis of mechanical- and corrosion-related degradation of carbon steel spent fuel container. Corrosion Engineering, Science and Technology, 49, 442–449.

Kotz J, Treichel P, Townsend J, 2008. Chemistry and Chemical reactivity. Vol 2. Boston: Cenage Learning.

Kursten B, Smailos E, Azkarate I, Werme L, Smart N R, Marx G, Cuñado M A and Santarini G, 2004. COBECOMA, State-of-the-art document on the corrosion behaviour of container materials. CONTRACT N° FIKW-CT-20014-20138 Final report, European Commission, Belgium.

Mason R M, Smith P N, Holton D, 2014. Modelling consequences of hypothetical criticality: Synthesis report for post-closure criticality consequence analysis. Report RWM 005140, Radioactive Waste Management, United Kingdom.

Navrotsky A, Mazeina L, Majzlan J, 2008. Size-driven structural and thermodynamic complexity in iron oxides. Science 319, 1635–1638.

Neff D, Dillman P, Descostes, M, Beranger G, 2006. Corrosion of iron archaeological artefacts in soil: estimation of average corrosion rates and thermodynamic calculations. Corrosion Science 48, 2947–2970.

Neff D, Saheb M, Monnier J, Perrin S, Descostes M, L´Hostis V, Cruset D, Millard A, Dillman P, 2010. A review of the archaeological analogue approaches to predict the long-term behaviour of carbon steel overpack and reinforced concrete structures in the French disposal system. Journal of Nuclear Materials 402, 196–205.

Pilling N B, Bedworth R E, 1923. The oxidation of metals at high temperature. The Japan Institute of Metals and Materials 29, 529–591.

Ronneteg U, 2023a. KBP3021 REBUS – Input parameters post-closure safety – Concept 1 version 3. SKBdoc 2024140 ver 1.0, Svensk Kärnbränslehantering AB.

Ronneteg U, 2023b. KBP3021 REBUS-Input parameters for post closure safety-Concept 1-P460N design. SKBdoc 2001895 ver 5.0, Svensk Kärnbränslehantering AB.

Saheb M, Neff D, Dillmann Ph, Mathiessen H, Foy E, 2008. Long term corrosion behaviour of low-carbon steel in anoxic environment: Characterization of archaeological artefacts. Journal of Nuclear Materials 379, 118–123.

Saheb M, Neff D, Dillmann Ph, Mathiessen H, Foy E, Bellot-Gurlet L, 2009. Multisecular corrosion behaviour of low carbon steel in anoxic soils: Characterisation of corrosion system on archaeological artefacts. Materials and Corrosion 60, 99–105.

Saheb M, Descostes M, Neff D, Mathiesen H, Michelin A, Dillmann P, 2010. Iron corrosion in anoxic soil: Comparison between thermodynamic modelling and ferrous artefacts characterized along with in situ geochemical conditions. Applied Geochemistry 25, 1937–1948.

Saheb M, Neff D, Bataillon C, Foy E, Dillmann P, 2011. Copper tracing to determine the micrometric electronic properties of a thick ferrous corrosion layer formed in an anoxic medium. Corrosion Science 53, 2201–2207.

Saheb M, Berger P, Raimbault L, Neff D, Dillmann P, 2012. Investigation of iron long term corrosion mechanism in anoxic media using deuterium tracing. Journal of Nuclear Materials 423, 61–66.

Sakuragi T, Yoshida S, Kinugasa J, Kato O, Tateishi Y, 2016. Corrosion kinetics of stainless steel by hydrogen measurement under deep geological repository condition. Proceedings of 42nd Annual Waste Management Conference, Phoenix, Arizona, 6–10 March 2016. Meza: WM Symposia Inc.

Sakuragi T, 2017. Report on corrosion behaviour of stainless steel. CAST-2017-D2.12, The European Atomic Energy Community, Luxembourg.

Salas J, Gimeno, M J, Auque L, Molinero J, Gimenez J, Juarez I, 2010. SR-Site hydrogeochemical evolution of the Forsmark site. SKB TR-10-58, Svensk Kärnbränslehantering AB.

Sidborn M, 2018. Metallic corrosion. SKBdoc 1622757 ver 1.0, Svensk Kärnbränslehantering AB.

SIS, 2013. SS-EN 10216-3. Seamless steel tubes for pressure purposes – Technical delivery conditions – Part 3: Alloy fine grain steel tubes. Stockholm: Swedish Standards Institute.

SIS, 2017. SS-EN 10028-2. Flat products made of steels for pressure purposes – Part 2: Nonalloy and alloy steels with specified elevated temperature properties. Stockholm: Swedish Standards Institute.

SIS, 2019. SS-EN 10025-2**.** Hot rolled products of structural steels – Part 2: Technical delivery conditions for non-alloy structural steels. Stockholm: Swedish Standards Institute.

Shoesmith D W, Zagidulin D, 2011. The corrosion of zirconium under deep geologic repository conditions. Journal of Nuclear Materials 418, 292–306.

Shoesmith D W, Taylor P, Bayley M G, Owen D G, 1980. The formation of ferrous monosulfide polymorfs during the corrosion of iron by aqueous hydrogen sulphide at 21 °C. Journal of Electrochemical Society 127, 1007–1015.

SKB, 2010. Design, production and initial state of the canister. SKB TR-10-14, Svensk Kärnbränslehantering AB.

SKB, 2022a. Post-closure safety for the final repository for spent nuclear fuel at Forsmark. Main report. PSAR version. SKB TR-21-01, Svensk Kärnbränslehantering AB.

SKB, 2022b. Fuel and canister process report, PSAR version. SKB TR-21-02, Svensk Kärnbränslehantering AB.

SKB, 2022c. Post-closure safety for the final repository for spent nuclear fuel at Forsmark. Data report, PSAR version. SKB TR-21-06, Svensk Kärnbränslehantering AB.

Smart N R, Adams R, 2006. Natural analogues for expansion due to the anaerobic corrosion of ferrous materials. SKB TR-06-44, Svensk Kärnbränslehantering AB.

Smart N R, Blackwood D J, Werme L O, 2001a. The anaerobic corrosion of carbon steel and cast iron in artificial groundwaters. SKB Technical Report TR-01-22, Svensk Kärnbränslehantering.

Smart N R, Bond A E, Crossley J A, Lovegrove P C and Werme L, 2001b. Mechanical properties of oxides formed by anaerobic corrosion of steel, MRS Symp. Proc. 663, pp. 477–485.

Smart N R, Blackwood D J, Werme L, 2002a. Anaerobic corrosion of carbon steel and cast iron in artificial groundwaters: Part 1-Electrochemical aspects. Corrosion 58, 547–559.

Smart N R, Blackwood D J, Werme L, 2002b. Anaerobic corrosion of carbon steel and cast iron in artificial groundwaters: Part 2-Gas generation. Corrosion 58, 627–637.

Smart N R, Rance A P and Werme L O, 2004. Anaerobic Corrosion of Steel in Bentonite. MRS Online Proceedings Library 807, 441–446.

Smart N R, Fennell P A and Rance A P, 2006a. Expansion due to the anaerobic corrosion of iron. SKB TR-06-41, Svensk Kärnbränslehantering AB.

Smart N R, Rance A P, Carlson L, Werme L O, 2006b. Further Studies of the Anaerobic Corrosion of Steel in Bentonite. MRS Online Proceedings Library 932, 813–820.

Smart N R, Bate F, Carlson L, Cave M R, Green K, Heath T G, Hoch A R, Hunter F M, Karnland O, Kemp S J, Milodowski A E, Olsson S, Pritchard A M, Rance A P, Shaw R A, Taylor H, Vickers B, Werme L, Williams C L, 2008. Interactions between iron corrosion products and bentonite. Deliverable 2.3.9 of EU-Project NF-PRO, May 2008, European Commission, Belgium.

Smart N R, Bond A E, Crossley J A, Lovegrove P C and Werme L, 2011. Mechanical properties of oxides formed by anaerobic corrosion of steel. MRS Online Proceedings Library 663, 477–485.

Smart N, Rance A, Reddy B, Fennell P, Winsley R, 2012. Analysis of SKB MiniCan Experiment 3. SKB TR-12-09, Svensk Kärnbränslehantering AB.

Smart N R, Reddy B, Rance A P, Nixon D J, Frutschi M, Bernier-Latmani R, Diomidis N, 2017. The anaerobic corrosion of carbon steel in compacted bentonite exposed to natural Opalinus Clay porewater containing native microbial populations. Corrosion Engineering, Science and Technology 52, 101–112.

Swanton S, Baston G and Smart N, 2015. Rates of steel corrosion and carbon-14 release from irradiated steel-state of the art review. CAST-2015-D2.1, European Commission, Belgium.

Winsley R J, Baldwin T D, Hicks T W, Mason R M, Smith P N, 2015. Understanding the likelihood and consequences of post-closure criticality in a geological disposal facility. Mineralogical Magazine 79, 1551–1561.

Yoshikawa H, Gunji E, Tokuda M, 2008. Long term stability of iron for more than 1 500 years indicated by archaeological samples from the Yamoto 6th tumulus. Journal of Nuclear Materials 379, 112–117.

Wada R, Nishimura T, Fujiwara K, Tanabe M and Mihara M, 1999. Experimental study on hydrogen gas generation rate from corrosion of Zircaloy and stainless steel under anaerobic alkaline conditions. Radioactive Waste Management and Environmental Remediation. The 7th International Conference Proceedings on Radioactive Waste Management and Environmental Remediations, Nagoya, 26–30 September, 1999. New York: ASME International.

Appendix A

Filling of the space outside fuel channels in BWR inserts

In the case of the Concept 1 BWR inserts for both steel grades it was noted early in this project that highly reactive configurations resulted when all the space outside the 12 fuel channels (Zircaloy boxes) was filled with corrosion products. This is mainly due to the unsymmetrical distribution of the free space in the BWR inserts, there is less in the 4 central compartments and more in the peripheral ones. This means that as corrosion proceeds, the corrosion layer will eventually contact the fuel channel from all sides in the central positions, while in the peripheral positions there is still free space. There are two possibilities for the surplus corrosion product in the central positions: it may enter the fuel channel and decrease the reactivity, or it may be transported to the peripheral positions where there is more free space. This second alternative, which results in higher reactivity, was assumed to occur in this study. To calculate the space outside the fuel channel in each compartment of the insert with a known volume (Table 5-4), the volume of the fuel assembly has to be estimated first.

The fuel channel of SVEA-96 Optima 3 is 140.2 mm on each side[14]. Thus, the volume inside the fuel channel is $0.1402 \times 0.1402 \times 4.460 = 0.08766$ m^3. This volume is in fact smaller because the fuel channel narrows to a cylinder + frustum of cones at the bottom 20 cm (transition piece), the assembly has a handle in the top 12 cm and is 4 cm shorter than the insert length. Based on the figures in Månsson[15] the sum of the 5 volumes of the transition piece (199 mm long) is 2.83 liters smaller than the fuel channel volume while the handle part is 118 mm long and together with the 40 mm shorter length has a volume of 3.1 liter. The steel details of the handle and bolts were assumed 1 liter (they may be more, but there is no easy way to calculate), so this part contributes 2.1 liter. Thus, the volume occupied by the assembly is $0.08766 \text{ m}^3 - 0.00493 \text{ m}^3 = 0.08273 \text{ m}^3$ or ~83 liters. This value will be used further below.

A1 BWR P355N insert

The free volume of this insert (see Figure 5-2 left) is different in the various compartments and is specified in Table 5-4 as: 0.102 m^3 the volume of each of the 4 central compartments, 0.120 m^3 is each of the 8 peripheric compartments. The total free volume of the insert is thus $4 \times (0.102) + 8 \times (0.120) = 1.368$ m^3. This means that in each of the 4 central positions the volume outside the fuel channel is $0.102 - 0.083 = 0.019$ m^3 or 19 litres. In the same way we have $0.120 - 0.083 = 0.037$ m^3 or 37 litres volume outside the fuel channel in each of the eight peripheric compartments. This means that the total free volume outside the 12 fuel channels is $4\ (0.019) + 8 \times (0.037) = 0.372$ m^3 or 372 litres.

In the case when the corrosion product is crystalline magnetite with $R_{P\text{-}B} = 2.1$, the volume of steel needed to corrode to fill the space outside the fuel channels (denoted X) is found by the relationship:

$$2.1 \times X = X + 0.372$$

which states that the volume of the corrosion product (left) should be equal to the initial free space outside the fuel channels plus the volume of the corrode iron (right).

It results that the free space outside the 12 fuel channels is filled with crystalline magnetite when a volume of 0.338 m^3 iron has corroded from a total internal surface of 53.39 m^2. This corresponds to the corrosion of $0.338 \text{ m}^3/53.39 \text{ m}^2 = 6.33 \times 10^{-3}$ m or 6.33 mm steel. It is clear that when the corrosion product is more voluminous, e.g., hydrated magnetite or corrosion product mixtures with $R_{P\text{-}B}$ values higher than 2.1, the filling of the space outside the fuel channels is achieved for less iron corroded.

[14] Söderberg H, 2004. Mekaniskt datablad för nukleär och termohydraulisk design O3 e21 SVEA-96 Optima 3. SKBdoc 1848330 ver 1.0. (Internal document, in Swedish.)

[15] Månson M, 2020. Final storage data SVEA-96 Optima F3-e34. SKBdoc 1900329 ver 1.0. (Internal document.)

A2 BWR P460N insert

The free volume of this insert (see Figure 5-4 left) is different in the various compartments and is specified in Table 5-4 as 0.106 m^3 for each of the 4 central compartments, 0.141 m^3 for each of the 4 peripheric side compartments and 0.120 m^3 for each of the 4 peripheric up and down compartments. This means that the free space outside the fuel channel with a volume of 0.083 m^3 in each compartment will be 0.106 − 0.083 = 0.023 m^3 or 23 litres in each central compartment, 0.141 − 0.083 = 0.058 m^3 or 58 litres in each peripheric side compartment and 0.120 − 0.083 = 0.37 m^3 or 37 litres in each peripheric up and down compartment. The total free volume outside the 12 fuel channels in the insert will be 4 × (0.023 + 0.058 + 0.037) = 0.472 m^3.

For crystalline magnetite with $R_{P\text{-}B}$ = 2.1 we have:

$$2.1 \times X = X + 0.472$$

From which follows X = 0.429 m^3 iron must corrode to fill all the space outside the 12 fuel channels. This will occur when 0.429 m^3/57.58 m^2 = 7.45×10^{-3} m or 7.45 mm iron corrodes. It is clear that for more voluminous iron corrosion products such as hydrated magnetite (Appendix B) or mixtures of anoxic corrosion products (Appendix C) the free space outside the fuel channels will be filled for less iron corroded.

Appendix B

Properties of hydrated magnetite

As discussed in Section 6.3.1 the corrosion product magnetite consists of two layers: a thin, strongly adherent layer and an outer porous layer of poor adhesion (Smart et al. 2002b). The adherent layer forms very quickly and does not increase further in thickness, while continuing corrosion leads to the thickening of the non-protective layer. As mentioned above, most of the magnetite produced in the non-protective layer is very probably some form of hydrated magnetite, less compact than crystalline magnetite, which contains different proportions of water in the structure. The thickness of the protective layer is reported to be less than 100 nm (Smart et al. 2006a), while the thinnest corrosion layer considered in this report corresponds to 1 mm carbon steel corroded producing e.g., 2.1 mm crystalline magnetite. By assuming the whole magnetite layer as hydrated magnetite we do not subtract the volume of the thin protective layer, but the error in the volume estimation is less than 0.005 %.

The mixture of magnetite with water can be calculated with water content in weight % or in volume %. The first alternative is discussed, i.e., weight percent.

a) Magnetite with 5 % weight water: the density is 4.26 g/cm^3, for a molecular formula of $Fe_3O_4 \cdot 0.68\ H_2O$, the molar weight is 243.72, the Pilling-Bedworth ratio is 2.68 (see next case for details of the calculation).

b) A sample of magnetite that contains 10 % weight water is made up of 90 g magnetite and 10 g water. The volume of 90 g magnetite is 90/5.17 g/cm^3 = 17.41 cm^3, while that of 10 g water is 10 cm^3. The total volume is 17.41 + 10 = 27.41 cm^3, while the total weight is 100 g. The density of this mixture is 3.65 g/cm^3. The calculation of the P-B ratio needs the calculation of molar weight.

   We have 90/231.53 = 0.3887 mol magnetite and 10/18 = 0.556 mol water, i.e. 1 mol magnetite contains 2.573 mol water and can be written $Fe_3O_4 \cdot 2.573\ H_2O$ with molar weight 277.88. With these values we have:

$$R_{PB} = \frac{V_{oxide}}{V_{metal}} = \frac{M_{oxide} \cdot \rho_{metal}}{n \cdot M_{metal} \cdot \rho_{oxide}} = \frac{277.88 \cdot 7.85}{3 \cdot 55.845 \cdot 3.65} = 3.57$$

   It already produces a large volume increase compared to crystalline magnetite and for this reason we have not assumed hydrated magnetite containing higher than 30 percent water.

c) For hydrated magnetite with 20 % water, we have: 80/5.17 = 15.47 cm^3 the volume of magnetite and 20 cm^3 water, resulting in a density of 100/35.47 cm^3 = 2.82 g/cm^3. For 80/231.53 = 0.3455 mol magnetite and 1.11 mol water, or $Fe_3O_4 \cdot 3.216\ H_2O$ with molecular weight 289.42 g/mol, the P-B ratio is 4.81.

d) For 30 percent water, we have 70/5.17 = 13.54 cm^3 magnetite volume and 30 cm^3 water, giving a density of 100/43.54 = 2.297 g/cm^3. For 70/231.53 = 0.302 mol magnetite and 1.667 mol water, or $Fe_3O_4 \cdot 5.52\ H_2O$ with molecular weight 330.89, the P-B ratio results 6.75. Such high P-B ratio would fill the canister quite quickly.

Initially we assumed this water ratio as the highest possible, based on the hydration number of the iron ion in water, i.e. $Fe(H_2O)_6$. A literature search on the subject suggests that the amount of water in the hydrated magnetite is lower than that, even though no direct measurements for hydrated magnetite could be found. In the literature, reference is made to $Fe_3O_4 \cdot 0.5\ H_2O$ as hydrated green magnetite or $Fe_3O_4 \cdot H_2O$ (Kotz et al. 2008). These water contents would correspond to 3.74 % respectively 7.2 % in weight of water. In the preparation of heavy concrete with hydrated magnetite as inert material (ACI 2007), the densities of such a material are reported in the range 4.2–4.8 gcm^{-3}. These densities for hydrated magnetite correspond approximately to magnetite with 5.54 % respectively 1.85 % in weight of water. The same source (ACI 2007) reports water contents of 12–18 % for hydrated Fe(III) oxides such as goethite and limonite, known to contain much more water than hydrated magnetite (Navrotsky et al. 2008).

During the review of this report, it was pointed out that such high contents of water would correspond to unreasonably high magnetite porosities and for this reason we have disregarded the data for magnetite with 20 % and 30 % water content. We considered necessary a reference in order to go even lower in water content, given the increase of reactivity hydrated magnetite causes in a filled insert (see Section 6.4.5).

Appendix C

Calculation of mixed anoxic corrosion products

As discussed in Section 6.3, a maximum of 1.8 moles siderite per year could be produced in each canister based on the groundwater composition in Forsmark. In the same way, assuming all sulphate converted to sulphide by SRB bacteria a maximum of 1.5 moles mackinawite per canister and year could be formed. The calculation is slightly different for the PWR and BWR insert which have different surface areas of steel corroding and different maximal reactivity configurations. In the case of a PWR insert the maximal reactivity configuration is achieved when the corrosion product layer touches the fuel rods, further corrosion causes a drastic decrease in reactivity when corrosion products substitute water between the fuel rods. In the case of a BWR insert the highest reactivity is achieved when the whole void outside the 12 fuel channels (Zircaloy boxes) is filled with corrosion products, but there is water between the fuel rods. Continued corrosion after this point in time causes corrosion products entering between the fuel rods which results in a drastic decrease of reactivity.

The total amount of iron corroded per year with a corrosion rate 1 μm/year is different for a PWR canister (27.71 m^2 surface for P355N and 39.07 m^2 for P460N) and a BWR canister (53.39 m^2 surface for P355N and 57.58 m^2 for P460N). Below the formation of siderite + magnetite and mackinawite + magnetite mixtures have been calculated separately for the P355N insert and P460N insert, first for the PWR case and then for the BWR case.

C1 PWR P355N canister

In this case 27.71 cm^3 iron corrodes per year by assuming a corrosion rate of 1 μm/year. This corresponds to 217.52 g Fe or 3.895 mol iron. In case the corrosion product is magnetite, 300.61 g magnetite is produced.

a) The first assumption is that out of the 3.895 mol Fe which corrodes per year, 1.8 mol Fe (1.8 × 55.845 = 100.52 g) give 208.54 g siderite as corrosion product, while 2.095 mol Fe (117 g) give 161.7 g magnetite. In total 370.24 g mixture is produced by the corrosion of 217.52 g Fe and it has a volume (for crystalline products) 208.54/3.87 = 53.89 cm^3 for siderite and 161.7/5.17 = 31.28 cm^3 for magnetite. The total volume of the mixture is thus 85.17 cm^3, i.e., the average density for the mixture is 4.35 g/cm^3. The weight percent of siderite in the mixture (siderite + magnetite) is 208.54/370.24 = 56.33 % siderite (rounded off to 56.3 %) while 43.7 % is magnetite. The simplest volume increase is calculated by the volume of Fe(s) (27.71 cm^3) and the volume of corrosion products which is 85.17 cm^3, i.e., $R_{P\text{-}B}$ = 85.17/27.71 = 3.07.

b) Another alternative, probably more possible to happen, is that the 1.8 moles of iron (100.52 g) give 1.8 moles of $FeCO_3$(s) corresponding to 208.54 g siderite, while the corrosion with magnetite formation continues with 1 μm/year all the time, i.e., the amount in gram of iron corroded this way is 217.52 g, giving 300.61 g magnetite. In total 509.15 g mixture siderite + magnetite is produced per year, with 40.96 weight percent siderite (208.54/509.15), rounded off to 41 %. The volumes of the corrosion products for crystalline solids are 53.89 cm^3 for siderite and 58.14 cm^3 for magnetite, in total 112.03 cm^3. The density of the mixture is 509.15 g/112.03 cm^3 = 4.54 g/cm^3. The volume increase is calculated from (100.52 + 217.52)/7.85 = 40.51 cm^3 Fe metal has given 112.03 cm^3 mixture siderite + magnetite, i.e., $R_{P\text{-}B}$ = 112.03/40.51 = 2.77.

c) In the case of mackinawite formation, according to the first assumption, out of the 3.895 mol Fe corroded, 1.5 mol (1.5 × 55.845 = 83.77 g) give 127.05 g mackinawite and 2.395 mol Fe (133.75 g) give 184.84 g magnetite. The total weight of corrosion products is 311.9 g while total volume 127.05/4.3 = 29.55 cm^3 mackinawite plus 35.75 cm^3 magnetite = 65.3 cm^3. The weight percent of mackinawite in the corrosion products is 127.05/311.9 = 40.7 % The average density of the corrosion product mixture is 311.9/65.3 = 4.78 g/cm^3. This gives a volume increase or P-B ratio of 65.3/27.71 = 2.36 for the case of crystalline products.

d) The alternative case here would be that 1.5 moles of sulphide as FeS are formed independently of the magnetite, which is formed with 1 μm/year (i.e., about 3.895 moles iron corroded per year to give magnetite). In case c) it was assumed that 3.895 moles Fe corrodes in total and out of this total amount, 1.5 moles corrode to give sulphide. In case d) the assumption is that since there is enough water, corrosion to give magnetite continues as usual and on top of this amount, 1.5 moles Fe corrode to give sulphide. The amount of sulphide is constrained by mass balance arguments.

In this case, 83.77 g iron corrode to give 127.05 g mackinawite each year, while 217.52 g iron corrode to give 300.61 g magnetite. In total 427.66 g mixture mackinawite + magnetite is formed, where mackinawite is 127.05/427.66 = 29.7 % in weight. The total volume of the mixture is 127.05/4.3 = 29.55 cm^3 mackinawite plus 300.61/5.17 = 58.14 cm^3 magnetite, in total 87.69 cm^3. The average density of the corrosion product mixture is 427.66/87.69 = 4.88 g/cm^3, and since 38.38 cm^3 iron is converted to 87.69 cm^3 mixture, the P-B ratio is thus 2.28. These data are summarized in Tables C-1 and C-2.

Table C-1. Data for case a) and c) of the mixed corrosion layer filling the gap.

Composition	Density (g/cm^3)	R_{P-B}	Corroded Fe (cm)	Corrosion layer (cm)
Fe_3O_4 100 %	5.17	2.1	0.865	1.817
a) $FeCO_3$ 56.3 % + Fe_3O_4 43.7 %	4.35	3.07	0.460	1.412
c) FeS 40.7 % + Fe_3O_4 59.3 %	4.78	2.36	0.700	1.652

Table C-2. Data for case b) and d) of the mixed corrosion layer filling the gap.

Composition	Density (g/cm^3)	R_{P-B}	Corroded Fe (cm)	Corrosion layer (cm)
Fe_3O_4 100 %	5.17	2.1	0.865	1.817
b) $FeCO_3$ 41 % + Fe_3O_4 59 %	4.54	2.77	0.538	1.490
d) FeS 29.7 % + Fe_3O_4 70.3 %	4.88	2.28	0.744	1.696

C2 PWR P460N canister

The surface area of this PWR insert is higher and in this case 39.07 cm^3 iron corrode per year by assuming a corrosion rate of 1 μm/year. This corresponds to 306.7 g Fe or 5.49 mol iron. In case the corrosion product is crystalline magnetite, 423.86 g magnetite is produced.

e) The first assumption is that out of the 5.49 mol Fe which corrodes per year, 1.8 mol Fe (1.8 × 55.845 = 100.52 g) give 208.54 g siderite as corrosion product, while 3.69 mol Fe (206.07 g) give 284.79 g magnetite. In total 493.33 g mixture are produced by the corrosion of 306.7 g Fe and they have a volume (for crystalline products) 208.54/3.87 = 53.89 cm^3 for siderite and 284.79/5.17 = 55.09 cm^3 for magnetite. The total volume for the mixture is 108.98 cm^3, i.e., the average density for the mixture is 493.33/108.98 = 4.53 g/cm^3. The weight percent of siderite in the mixture (siderite + magnetite) is 208.54/493.33 = 42.27 % siderite while the rest is magnetite. The simplest volume increase is calculated by the volume of Fe(s) (39.07 cm^3) and the volume of corrosion products which is 108.98 cm^3, i.e., R_{P-B} = 108.98/39.07 = 2.79.

f) Another alternative, probably more possible to happen in reality, is that the 1.8 moles of iron (100.52 g) give 1.8 moles of $FeCO_3$(s) corresponding to 208.54 g siderite, while the corrosion with magnetite formation continues with 1 μm/year all the time, i.e., the amount in gram of iron corroded this way is 306.7 g, giving 423.86 g magnetite. In total 623.4 g mixture siderite + magnetite is produced per year, with 33.45 weight percent siderite (208.54/623.4). The volumes of the corrosion products for crystalline solids are 53.89 cm^3 for siderite and 81.98 cm^3 for magnetite, in total 135.87 cm^3. The density of the mixture is 623.4 g/135.87 cm^3 = 4.59 g/cm^3. The volume increase is calculated from (100.52 + 306.7)/7.85 = 51.88 cm^3 Fe metal has given 135.87 cm^3 mixture siderite + magnetite, i.e. R_{P-B} = 135.87/51.88 = 2.62.

g) In the case of mackinawite formation, according to the first assumption, out of the 5.49 mol Fe corroded, 1.5 mol (1.5 × 55.845 = 83.77 g) give 127.05 g mackinawite and 3.99 mol Fe (222.82 g) give 307.94 g magnetite. The total weight of corrosion products is 434.99 g while the total volume is 127.05/4.3 = 29.55 cm^3 mackinawite plus 59.56 cm^3 magnetite = 89.11 cm^3. The weight percent of mackinawite in the corrosion products is 127.05/434.99 = 29.21 % The average density of the corrosion product mixture is 434.99/89.11 = 4.88 g/cm^3. This gives a volume increase or P-B ratio of 89.11/39.07 = 2.28 for the case of crystalline products.

h) The alternative case here would be that 1.5 moles of sulphide as FeS are formed independently of the magnetite, which is formed with 1 µm/year (i.e., about 5.49 moles iron corroded per year to give magnetite). In case c) it was assumed that 5.49 moles Fe corrodes in total and out of this total amount, 1.5 moles corrode to give sulphide. In case d) the assumption is that since there is enough water, corrosion to give magnetite continues as usual and on top of this amount, 1.5 moles Fe corrode to give sulphide. The amount of sulphide is constrained by mass balance arguments.

In this case, 83.77 g iron corrode to give 127.05 g mackinawite each year, while 306.7 g iron corrode to give 423.86 g magnetite. In total 550.91 g mixture mackinawite + magnetite are formed, where mackinawite is 127.05/550.91 = 23.06 % in weight. The total volume of the mixture is 127.05/4.3 = 29.55 cm^3 mackinawite plus 423.86/5.17 = 81.98 cm^3 magnetite = 111.53 cm^3. The average density of the corrosion product mixture is 550.91/111.53 = 4.94 g/cm^3, and since 49.74 cm^3 iron is converted to 111.53 cm^3 mixture, the P-B ratio is thus 2.24. The data for the insert PWR P460N are summarized in Tables C-3 and C-4.

Table C-3. Data for case e) and g) of the mixed corrosion layer filling the gap.

Composition	Density (g/cm^3)	R_{P-B}	Corroded Fe (cm)	Corrosion layer (cm)
Fe_3O_4 100 %	5.17	2.1	0.747	1.569
e) $FeCO_3$ 42.3 % + Fe_3O_4 57.7 %	4.53	2.79	0.459	1.281
g) FeS 29.2 % + Fe_3O_4 70.8 %	4.88	2.28	0.642	1.464

Table C-4. Data for case f) and h) of the mixed corrosion layer filling the gap.

Composition of corrosion products	Density (g/cm^3)	R_{P-B}	Corroded Fe (cm)	Corrosion layer (cm)
Fe_3O_4 100 %	5.17	2.1	0.747	1.569
f) $FeCO_3$ 33.5 % + Fe_3O_4 66.5 %	4.59	2.62	0.507	1.329
h) FeS 23 % + Fe_3O_4 77 %	4.94	2.24	0.642	1.464

C3 BWR P355N canister

The total surface area of this insert is 53.39 m^2, meaning that with a corrosion rate of 1 µm/year, 53.39 cm^3 iron (or 419.11 g iron or 7.505 mol iron) is corroded each year and in case only magnetite is formed, 579.22 g magnetite is produced each year.

i) The assumption in the first case is that out of the 7.505 mol Fe which corrodes per year, 1.8 mol Fe (1.8 × 55.845 = 100.52 g) give 208.54 g siderite as corrosion product while the rest, 5.705 mol Fe (318.6 g) give 440.3 g magnetite. In total 648.84-gram mixture is produced by the corrosion of 419.11 g Fe and it has a volume (for crystalline products) 208.54/3.87 = 53.89 cm^3 for siderite and 440.3/5.17 = 85.16 cm^3 for magnetite. The total volume for the mixture is 139.05 cm^3, i.e., the average density for the mixture is 4.67 g/cm^3. The weight percent of siderite in the mixture siderite + magnetite is 208.54/648.84 = 32.1 % siderite and 67.9 % is magnetite. The simplest volume increase is calculated by the volume of Fe(s) (53.39 cm^3) and the volume of corrosion products is 139.05 cm^3, i.e., R_{P-B} = 139.05/53.39 = 2.60.

j) The other alternative, probably more possible to happen, is that the 1.8 moles of iron (100.52 g) give 1.8 moles of $FeCO_3$(s) corresponding to 208.54 g siderite, while the corrosion with magnetite formation continues with 1 µm/year all the time, i.e., the amount in gram of iron corroded this way is 419.11 g, giving 579.22 g magnetite. In total 787.76 g mixture siderite + magnetite is produced per year, with 26.5 weight percent siderite (208.54/787.76). The volumes of the corrosion products for crystalline solids are 53.89 cm^3 for siderite and 112.03 cm^3 for magnetite, in total 165.92 cm^3. The density of the mixture is 787.76 g/165.92 cm^3 = 4.75 g/cm^3. The volume increase is calculated from (100.52 + 419.11)/7.85 = 66.19 cm^3 Fe metal has given 165.92 cm^3 mixture siderite + magnetite, i.e. R_{P-B} = 2.51.

k) In the case of mackinawite formation, according to the first assumption, out of the 7.505 mol Fe corroded, 1.5 mol (1.5 × 55.845 = 83.77 g) give 127.05 g mackinawite and 6 mol Fe (335.35 g) give 463.45 g magnetite. The total weight of corrosion products is 590.5 g while the total volume is 127.05/4.3 = 29.55 cm^3 mackinawite plus 89.64 cm^3 magnetite, in total 119.19 cm^3. The weight percent of mackinawite in the corrosion products is 127.05/590.5 = 21.5 %. The average density of the corrosion product mixture is 590.5/119.19 = 4.95 g/cm^3. The volume increase or P-B ratio is found from the ratio of the volume of corrosion products to this of iron corroded, 119.19/53.39 = 2.23 for the case of crystalline products.

l) The alternative case here would be that 1.5 moles of sulphide as FeS are formed independently of the magnetite, which is formed with 1 μm/year (i.e., about 7.505 moles iron are corroded per year to give magnetite). In this case the assumption is that since there is enough water, corrosion to give magnetite continues as usual and on top of this amount, 1.5 moles Fe corrode to give sulphide.

In this case, 83.77 g iron corrodes to give 127.05 g mackinawite each year, while 419.11 g iron corrode to give 579.22 g magnetite. In total, 706.27 g mixture of mackinawite + magnetite is formed, where mackinawite is 127.05/706.27 = 18 % in weight. The volume of the corrosion product mixture is 127.05/4.3 = 29.55 cm^3 mackinawite and 579.22/5.17 = 112.03 cm^3 magnetite, in total 141.58 cm^3 mixture. The average density of the corrosion product mixture is 706.27/141.58 = 4.99 g/cm^3, and since 64.06 cm^3 iron is converted to 141.58 cm^3 mixture, the P-B ratio is thus 2.21.

Below are Tables C-5 and C-6 with data calculated for the case when corrosion product mixtures fill completely the space outside the 12 fuel channels in the BWR P355N insert for the different corrosion product mixtures.

The total free volume outside the fuel channels in the insert BWR P355N is 0.372 m^3 (see Appendix A). Let's first calculate the volume of iron (denoted X) that should corrode to fill this space with pure crystalline magnetite, which has $R_{P\text{-}B}$ = 2.1. From the relation 2.1 × X = X + 0.372, which relates the volume of corrosion product produced on the left with the initial free space (0.372 m^3) and the volume of iron corroded (X), it results that 0.338 m^3 iron should corrode from a surface of 53.39 m^2 to fill all the free space outside fuel channels. This corresponds to the corrosion of 0.338/53.39 = 6.33 mm iron. The framework plates will have corroded 12.7 mm (6.33 on each side) and 19.3 mm steel is uncorroded on each plate of total initial thickness 32 mm, while in the thick corner plates remains much more steel uncorroded.

In case **i),** the filling of the 0.372 m^3 volume outside the fuel channels with the mixture of 32.1 % siderite and 67.9 % magnetite can be found from R_{PB} = 2.60, thus 2.60 × X = X + 0.372 which gives X = 0.2325 m^3 Fe needs to corrode to fill all the space outside fuel channels with this mixture. This means that 0.2325/53.39 = 4.35 10^{-3} m or 4.35 mm iron needs to corrode in this case. Similar calculations for the other cases are summarized in Tables C-5 and C-6.

Table C-5. Data for case i) and k) of the mixed corrosion layer which fills the space outside 12 fuel channels.

Composition of corrosion products	Density (g/cm^3)	$R_{P\text{-}B}$	Corroded Fe (cm)
Fe_3O_4 100 %	5.17	2.1	0.633
i) $FeCO_3$ 32.1 % + Fe_3O_4 67.9 %	4.67	2.60	0.435
k) FeS 21.5 % + Fe_3O_4 78.5 %	4.95	2.23	0.566

Table C-6. Data for case j) and l) of the mixed corrosion layer which fills the space outside the 12 fuel channels.

Composition of corrosion products	Density (g/cm^3)	$R_{P\text{-}B}$	Corroded Fe (cm)
Fe_3O_4 100 %	5.17	2.1	0.633
j) $FeCO_3$ 26.5 % + Fe_3O_4 73.5 %	4.75	2.51	0.461
l) FeS 18 % + Fe_3O_4 82 %	4.99	2.21	0.576

C4 BWR P460N canister

The total surface area of this insert is 57.58 m^2, meaning that with a corrosion rate of 1 µm/year, 57.58 cm^3 iron (or 452.0 g iron, or 8.09 mol iron) is corroded each year and in case only magnetite is formed, 624.67 g magnetite is produced each year.

m) The assumption in the first case is that out of the 8.09 mol Fe which corrodes per year, 1.8 mol Fe (1.8 × 55.845 = 100.52 g) give 208.54 g siderite as corrosion product while the rest, 6.29 mol Fe (351.27 g) give 485.45 g magnetite. In total 693.99-gram mixture is produced by the corrosion of 452.0 g Fe and it has a volume (for crystalline products) 208.54/3.87 = 53.89 cm^3 for siderite and 485.45/5.17 = 93.90 cm^3 for magnetite. The total volume for the mixture is 147.79 cm^3, i.e., the average density for the mixture is 4.7 g/cm^3. The weight percent of siderite in the mixture siderite + magnetite is 208.54/693.99 = 30.0 % siderite, and the rest is magnetite. The simplest volume increase is calculated by the volume of Fe(s) (57.58 cm^3) and the volume of corrosion products which is 147.79 cm^3, i.e., $R_{P\text{-}B}$ = 140.32/54 = 2.57.

n) The other alternative, probably more possible to happen in reality, is that the 1.8 moles of iron (100.52 g) give 1.8 moles of $FeCO_3$(s) corresponding to 208.54 g siderite, while the corrosion with magnetite formation continues with 1 µm/year all the time, i.e., the amount in gram of iron corroded this way is 452.0 g, giving 624.67 g magnetite. In total 833.21 g mixture siderite + magnetite is produced per year, with 25.03 weight percent siderite (208.54/833.21). The volumes of the corrosion products for crystalline solids are 53.89 cm^3 for siderite and 120.83 cm^3 for magnetite, in total 174.72 cm^3. The density of the mixture is 833.21 g/174.72 cm^3 = 4.77 g/cm^3. The volume increase is calculated from (100.52 + 452.0)/7.85 = 70.38 cm^3 Fe metal has given 174.72 cm^3 mixture siderite + magnetite, i.e. $R_{P\text{-}B}$ = 2.48.

o) In the case of mackinawite formation, according to the first assumption, out of the 8.09 mol Fe corroded, 1.5 mol (1.5 × 55.845 = 83.77 g) give 127.05 g mackinawite and 6.59 mol Fe (368.02 g) give 508.6 g magnetite. The total weight of corrosion products is 635.65 g while the total volume is 127.02/4.3 = 29.54 cm^3 for mackinawite plus 98.38 cm^3 magnetite, in total 127.92 cm^3. The weight percent of mackinawite in the corrosion products is 127.05/635.65 = 20.0 %. The average density of the corrosion product mixture is 635.65/127.92 = 4.97 g/cm^3. This gives a volume increase or P-B ratio of 127.92/57.58 = 2.22 for the case of crystalline products.

p) The alternative case here would be that 1.5 moles of sulphide as FeS are formed independently of the magnetite, which is formed with 1 µm/year (i.e. about 8.09 moles iron are corroded per year to give magnetite). In this case the assumption is that since there is enough water, corrosion to give magnetite continues as usual and on top of this amount, 1.5 moles Fe corrode to give sulphide.

In this case, 83.77 g iron corrodes to give 127.05 g mackinawite each year, while 452.0 g iron corrode to give 624.67 g magnetite. In total, 751.72 g mixture of mackinawite + magnetite is formed, where mackinawite is 127.05/751.72 = 16.9 % in weight. The volume of the corrosion product mixture is 127.05/4.3 = 29.55 cm^3 mackinawite and 624.67/5.17 = 120.83 cm^3 magnetite, in total 150.38 cm^3 mixture. The average density of the corrosion product mixture is 751.72/150.38 = 5.00 g/cm^3, and since 68.25 cm^3 iron is converted to 150.38 cm^3 mixture, the P-B ratio is thus 2.20.

As discussed in Appendix A, the configuration with the highest reactivity in a BWR insert is achieved when all the free volume outside of the 12 fuel channels is filled with corrosion products, but there is still water inside the fuel channel. For the BWR P460N insert the free volume outside the fuel channels 0.472 m^3 (see Appendix A) while the total steel surface is 57.58 m^2. The free volume outside the 12 fuel channels is filled with crystalline magnetite when 7.45 mm iron has corroded, which corresponds to a volume of 0.00745 m × 57.58 m^2 = 0.429 m^3 iron. This produces 0.429 × 2.1 = 0.901 m^3 magnetite which fills the free volume (0.472 m^3) plus the volume of the corroded iron (0.429 m^3), 0.472 + 0.429 = 0.901 m^3.

In the other cases with corrosion product mixtures (or hydrated magnetite), which have different volume increases (or $R_{P\text{-}B}$), the volume of iron (denoted X) needed to corrode to fill the space outside the fuel channels is found from the relation:

$$R_{P\text{-}B} \times X = X + 0.472$$

Thus, for case **m)** above with a mixture composed of 30 % siderite and 70 % magnetite, which has R_{PB} = 2.57, X = 0.472/1.57 = 0.3006 m^3, from which the corrosion depth is calculated by dividing with the total surface: 0.3006 m^3/57.58 m^2 = 5.22 10^{-3} m or 5.22 mm. The corrosion product mixture is more voluminous than crystalline magnetite ($R_{P\text{-}B}$ = 2.57 instead of 2.1), hence the free volume outside the 12 fuel channels is filled after the corrosion of 5.22 mm carbon steel instead of 7.45 mm needed to fill the same free space with crystalline magnetite. In Tables C-7 and C-8 the corrosion product mixture compositions, density, R_{PB} and the depth of steel needed to corrode to fill all the space outside the 12 fuel channels are summarized.

Table C-7. Data for case m) and o) of the mixed corrosion layer which fills the space outside the fuel channels.

Composition of corrosion products	Density (g/cm^3)	$R_{P\text{-}B}$	Corroded Fe (cm)
Fe_3O_4 100 %	5.17	2.1	0.745
m) $FeCO_3$ 30 % + Fe_3O_4 70 %	4.70	2.57	0.522
o) FeS 20.0 % + Fe_3O_4 80.0 %	4.97	2.22	0.672

Table C-8. Data for case n) and p) of the mixed corrosion layer which fills the space outside the fuel channels.

Composition of corrosion products	Density (g/cm^3)	$R_{P\text{-}B}$	Corroded Fe (cm)
Fe_3O_4 100 %	5.17	2.1	0.745
n) $FeCO_3$ 25 % + Fe_3O_4 75 %	4.77	2.48	0.554
p) FeS 16.9 % + Fe_3O_4 83.1 %	5.00	2.20	0.683

Arkitektkopia AB, Bromma, 2024

SKB is responsible for managing spent nuclear fuel and radioactive waste produced by the Swedish nuclear power plants such that man and the environment are protected in the near and distant future.

skb.se